Two classes of chromatin domains are important for fidelity of human centromeres

Daniël P. Melters[1,*], Tatini Rakshit[1,*], Minh Bui[1], Sergei A. Grigoryev[2], David Sturgill[1], and Yamini Dalal[1,#]

1 National Cancer Institute, Center for Cancer Research, Laboratory of Receptor Biology and Gene Expression, Bethesda, MD

2 Pennsylvania State University, College of Medicine, Hershey, PA

* Contributed equally

Corresponding author: dalaly@mail.nih.gov

Keyword: chromosome, mitosis, kinetochore, nucleosomes, chromatin, centromere

Abstract

The centromere is a vital locus on each chromosome which seeds the kinetochore, allowing for a physical connection between the chromosome and the mitotic spindle. At the heart of the centromere is the centromere-specific histone H3 variant CENP-A/CENH3. Throughout the cell cycle the constitutive centromere associated network is bound to CENP-A chromatin, but how this protein network modifies CENP-A nucleosome dynamics *in vivo* is unknown. Here, using a combination of biophysical and biochemical analyses we provide evidence for the existence of two populations of CENP-A nucleosomes that co-exist at human centromeres. Disrupting the balance of these two populations by overexpressing CENP-C results in reduced levels of centromeric RNA polymerase 2, impair *de novo* CENP-A loading, and correlate with significant

mitotic defects. Mutants that either serve as a sink for excess CENP-C, or which are unable to bind CENP-C rescue the mitotic defects. These data support a model where a balance between both CENP-A populations is required for mitotic fidelity.

Introduction

The kinetochore is a large proteinaceous complex which physically connects centromeric chromatin to the mitotic microtubule spindles. Inaccuracies in kinetochore assembly can lead to the formation of dicentric chromosomes, or chromosomes lacking kinetochores. In either case, chromosomes fail to segregate faithfully, which drives genomic instability. Electron microscopy studies of mitotic centromeres reveal a two-layered electron dense structure that is over 200 nm in width and over 50 nm in depth (Comings and Okada, 1970; Rattner *et al.*, 1975; Esponda, 1978; McEwen *et al.*, 1998), delineated into the inner and outer kinetochore.

At the base of the inner kinetochore is the histone H3 variant CENP-A (CENH3), which is marked by its rapid evolution (Malik and Henikoff, 2001, 2003; Cooper and Henikoff, 2004; Talbert *et al.*, 2004; Meraldi *et al.*, 2006; Maheshwari *et al.*, 2015), and its association with equally rapid evolving centromere DNA (Melters *et al.*, 2013). This enhanced rate of evolution of sequences underlying the essential and conserved function is commonly referred to as the centromere paradox (Henikoff *et al.*, 2001). Nevertheless, despite lack of sequence conservation at the level of CENP-A, and its associated DNA, in most species, CENP-A chromatin provides the epigenetic and structural foundation to assemble the kinetochore, recruiting inner kinetochore proteins CENP-B, CENP-C, and CENP-N (Regnier *et al.*, 2005; Mendiburo *et al.*, 2011). Together, these inner kinetochore components provide recognition motifs for outer kinetochore

proteins in the conserved KMN network (KLN1, MIS12 and NDC80 complexes (Cheeseman *et al.*, 2006; Przewloka *et al.*, 2007; DeLuca and Musacchio, 2012; Weir *et al.*, 2016). Deleting either CENP-A or CENP-C results in cell death or senescence (Fukagawa *et al.*, 1999; Kwon *et al.*, 2007; McKinley and Cheeseman, 2016), but this happens only after a few cell cycles. These data indicate that both CENP-A and CENP-C are often present in excess for what is required to form a functional kinetochore for one cell cycle. Furthermore, CENP-A and CENP-C are long lived proteins guaranteeing faithful chromosome segregation even after their respective genes have been deleted (Howman *et al.*, 1999; Kalitsis *et al.*, 2002; Suzuki *et al.*, 2011; Bodor *et al.*, 2013; Smoak *et al.*, 2016).

Despite major advances made in understanding the hierarchy of the centromere and kinetochore proteins (Milks *et al.*, 2009; Cheeseman, 2014; Klare *et al.*, 2015; McKinley and Cheeseman, 2016), little is known about the physical features of the inner kinetochore bound to centromeric chromatin in multicellular eukaryotes. Individual mitotic kinetochores were isolated from budding yeast by using a FLAG-tagged outer kinetochore component Dsn1 as bait (Gonen *et al.*, 2012). Point centromeres of budding yeast are unique because they display a one-to-one correspondence, in which a single CENP-A containing nucleosome (Bloom and Carbon, 1982; Saunders *et al.*, 1988; Furuyama and Henikoff, 2009; Kingston *et al.*, 2011; Krassovsky *et al.*, 2011; Furuyama *et al.*, 2013; Henikoff *et al.*, 2014; Díaz-Ingelmo *et al.*, 2015) binds to a single microtubule via the kinetochore. In contrast, the human centromeres are regional centromeres comprised of megabase-sized α-satellite arrays (Rudd *et al.*, 2006; Waye and Willard, 2006). Recent advances in super resolution microscopy suggest that each human centromere harbors ~400 CENP-A molecules (Bodor *et al.*, 2014), which eventually associate with only ~17 mitotic

microtubule spindles (Suzuki *et al.*, 2015). This inner kinetochore chromatin is thought to be folded into a boustrophedon (Ribeiro *et al.*, 2010; Vargiu *et al.*, 2017), in which the number of CENP-A nucleosomes present appears to exceed the number needed for centromere function. Thus, in order to uncover physical properties that define the regional centromere, it is of interest to purify chromatin associated with the inner kinetochore from human cells.

In this report, using nanoscale and immunofluorescence imaging, and biochemical approaches, we report on two classes of CENP-A chromatin populations in human cells. One class of CENP-A nucleosomes is weakly associated with inner kinetochore proteins and possesses diminutive dimensions; whereas a second class of CENP-A nucleosomes co-elute and co-purify with inner kinetochore proteins, and display octameric dimensions. Overexpression of CENP-C alters the balance of these two CENP-A classes, resulting in reduced RNA polymerase 2 occupancy, reduced *de novo* loading of CENP-A nucleosomes, and extensive mitotic defects. CENP-A mutants that either serve as a sink for excess CENP-C or which are unable to bind CENP-C rescue these mitotic defects. Altogether, these data support a model where the existence of two classes of centromeric chromatin are required for centromere fidelity.

Results

Two distinct classes of centromeric chromatin can be purified from human centromeres

In previous work, we purified human CENP-A nucleosomes under a range of conditions, and analyzed them by various biochemical, EM and AFM approaches (Dimitriadis *et al.*, 2010; Bui *et al.*, 2012). We occasionally noticed a small fraction of macromolecular complexes within CENP-A native chromatin-immunoprecipitation (N-ChIP), that were large, compacted, and

refractory to standard nucleosome analysis (Dimitriadis *et al.*, 2010; Bui *et al.*, 2012). We were curious to examine whether such larger complexes might represent the intact inner kinetochore complex. Therefore, we developed a gentle, native, serial chromatin-immunoprecipitation assay to purify CENP-C bound chromatin from HeLa cells (Supplemental Figure S1). We mildly digested nuclear chromatin with micrococcal nuclease (MNase), and performed N-ChIP by first pulling-down CENP-C bound chromatin and subsequent pulling-down any remaining CENP-A chromatin using ACA serum (Earnshaw and Rothfield, 1985) (Figure 1A).

We used quantitative immunoblotting to quantify the relative abundance of native CENP-A bound to CENP-C (Figure 1B) and free CENP-A chromatin. The enrichment of the N-ChIP'ed samples was measured over the input. We observed a 2.0±0.8-fold enrichment of CENP-A in the CENP-C N-ChIP and an 8.5±2.8-fold enrichment of CENP-A in the serial ACA N-ChIP (Figure 1C). Thus, our results indicate that in HeLa cells, there is a ~4.7-fold excess of CENP-A that is not strongly associated with CENP-C.

To test the possibility that during the experimental procedure of N-ChIP, CENP-C dissociates from CENP-A chromatin, we also cross-linked samples prior to ChIP. Although in our hands overall chromatin extraction efficiency is generally lower under X-ChIP conditions, we observed a 2.5±0.9-fold enrichment of CENP-A in the CENP-C X-ChIP and a 7.5±3.7-fold enrichment of CENP-A in the ACA X-ChIP (Figure 1C, Supplemental Figure S1E, Table S1).

We next tested the possibility that CENP-C may be dissociating from one class of CENP-A chromatin. In this scenario, the additional CENP-C would accumulate in the nuclear pellet. To

examine how much CENP-C is lost during purification, we loaded a gradient of nuclear extract in addition to the serial N-ChIP (Figure 1D). We found that very little CENP-C remained in the pellet. These data lend confidence to the interpretation that the majority of CENP-C was pulled-down in the CENP-C N-ChIP.

Next, we tested whether the two types of CENP-A populations have similar sedimentation patterns. Following MNase digestion, we ran the chromatin on a 5-20% glycerol gradient and performed serial N-ChIP on both every fraction (Supplemental Figure S2A). Whereas the free CENP-A population had a sedimentation pattern very similar to input, CENP-C associated CENP-A chromatin showed a distinctively different sedimentation pattern (Supplemental Figure S2). The relative abundance of longer chromatin arrays in the CENP-C N-ChIP was also observed by high resolution capillary electrophoresis (BioAnalyzer, Supplemental Figure S3). We were curious to test whether CENP-C-associated chromatin occupied unique centromeric sequences compared to CENP-C-depleted CENP-A chromatin. Through ChIP-seq analysis we showed that both CENP-A populations occupy essentially similar centromeric sequences (Supplemental Figure S4).

Altogether, these data suggest that there is a sizeable fraction of CENP-A chromatin which is weakly associated with CENP-C, but a smaller fraction of CENP-A which is very robustly bound to CENP-C at the human centromere.

CENP-A nucleosomes robustly bound to CENP-C co-purify with other CCAN components

The chromatin we extracted is from cycling HeLa cells, the majority of which are in G1 phase (Pettersen *et al.*, 1977). Throughout the cell cycle the constitutive centromere associated network (CCAN) complex, which is composed of several proteins, is bound to the centromeric chromatin to form the inner kinetochore (Figure 2A) (McKinley and Cheeseman, 2016; Pesenti *et al.*, 2016). To test whether other components of the CCAN are present within the complex within CENP-A:CENP-C above, we performed western blot analyses on these purified CENP-C complexes. In addition to CENP-A, H2A, and H2B, CCAN components CENP-B, CENP-I, CENP-N, CENP-W, and CENP-T were enriched (Figure 2B). To our surprise, the dedicated chaperone for CENP-A assembly, HJURP was also enriched in the CENP-C N-ChIP. This result is consistent with a recent report from BioID experiments showing that HJURP is associated with CENP-A chromatin at multiple points of the cell cycle (Remnant *et al.*, 2019). Overall, our purified CENP-A:CENP-C complex robustly represents the CCAN. Furthermore, outer kinetochore components MIS12 and HEC1/NDC80 were modestly enriched in the CENP-C N-ChIP (Figure 2B). Altogether, from these data, we deduced that the large CENP-C complex that was enriched in fraction 12 of our glycerol gradient experiments (Supplemental Figure S2D) includes the full CCAN, possibly representing fully matured kinetochores.

Inner kinetochore associated chromatin is not uniquely enriched in histone H2A variants

Heterotypic CENP-A/H3.3 nucleosomes have been reported, they are generally restricted to ectopic sites (Lacoste *et al.*, 2014; Athwal *et al.*, 2015; Nye *et al.*, 2018). Where histone H3 and H2B have few variants, there are several histone H2A variants including macroH2A, H2A.Z, and γH2A.X (Melters *et al.*, 2015). Indeed, mass-spectrometry data has suggested that H2A histone variants might form nucleosomes with CENP-A (Foltz *et al.*, 2006; Bailey *et al.*, 2016). We

therefore set out to interrogate the possibility that CENP-A nucleosomes associated with the inner kinetochore contained other histone variants. As before, we performed a CENP-C N-ChIP followed by a serial ACA N-ChIP and tested both samples for the presence of histone H2A variants. Interestingly, while we detected H2A.Z and macroH2A variants in both CENP-C and ACA N-ChIP (Figure 2C), their relative abundance was not quantifiably different between the two CENP-A populations (Figure 2D, Supplemental Table S2). Consequently, these data do not currently provide evidence that H2A variants might contribute to structural differences between the two CENP-A populations.

Immuno-AFM confirms presence of CENP-A nucleosomes associated with the CENP-C complex

The purification of CENP-A chromatin bound to the full CCAN from human cells present an opportunity to describe its features and properties. In order to do this, we first set out to confirm the identity of nucleosomes associated with CENP-C using an independent visual approach, complementary to the Western blot analyses provided above (Figures 1, S2). To this end, we developed a single-molecule based method to test whether CENP-A nucleosomes are physically present in CENP-C N-ChIP samples. Inspired by classical immuno-EM protocols and recognition-AFM (Wang *et al.*, 2008), in which one can confirm the identity of a given molecule in a biological sample, we adapted immuno-labeling for in-air atomic force microscopy (AFM) (Figure 3A). We first visualized samples either without antibody; or, primary (1^{o}) mouse monoclonal anti-CENP-A antibody; or, 1^{o} CENP-A antibody and, either secondary (2^{o}) anti-mouse antibody or 2^{o} anti-mouse Fab fragment. The 1^{o} antibody by itself was 0.8±0.2 nm in height and the addition of the 2^{o} antibody resulted in a height increase to 2.0±0.5 nm (Figures

3B, C, Supplemental Table S3, Raw Data File 1). To confirm the 1° antibody's specificity, we used *in vitro* reconstituted recombinant H3 or CENP-A nucleosomes as before and incubated them with either no antibody (no Ab); 1° alone, or 1° + 2° antibodies, respectively (Figures 3B, C). As expected, control *in vitro* reconstituted H3 nucleosomes did not show a shift in particle height in the presence of anti-CENP-A antibodies (no Ab: 2.2±0.2nm, 1°: 2.1±0.2 nm, and 2°: 2.2±0.1 nm, resp.). However, *in vitro* reconstituted CENP-A nucleosomes did increase in height upon binding to their antibodies (no Ab: 2.2±0.2 nm, 1°: 2.5±0.3 nm, and 4.6±1.4 nm with 2° antibody, or 3.2±0.6 nm with Fab fragment, resp., Figures 3B, C, S5, Supplemental Table S3, Raw Data File 1).

Having standardized this approach on *in vitro* reconstituted samples, we next applied this method to *in vivo* samples, namely native H3 or CENP-C purified chromatin (Figures 3B, C). Similar to reconstituted H3 nucleosomes, native bulk H3 chromatin did not demonstrate a shift in particle height when incubated with anti-CENP-A antibodies (no Ab: 2.3±0.2 nm, 1°: 2.4±0.3 nm, and 2°: 2.3±0.1 nm, resp.). In contrast, nucleosomal particles that came down in the CENP-C N-ChIP displayed a shift in height when challenged with anti-CENP-A antibodies (no Ab: 2.4±0.4 nm, 1°: 2.6±0.4 nm, and 2°: 3.9±1.3 nm, resp.). These results support the biochemical interpretation that CENP-A nucleosomes are associated with the purified CENP-C complex.

Physically altered CENP-A nucleosomes are bound to the inner kinetochore

We were excited to analyze physical characteristics of purified CCAN associated CENP-A chromatin, which to our knowledge, has not been accomplished before. In order to image these complexes, we split the samples in half, and imaged the same samples independently (by two

different operators) using complementary high resolution single-molecule methods: in-air AFM; and transmission electron microscopy (TEM) (Figures 4A, B, S6). By AFM and TEM, we observed large polygonal structures with a roughly circular footprint (height: 5.8±2.1 nm; area: 629±358 nm^2) associated with four to six nucleosomes (Figures 4A, B, S6, Table S4, Raw Data File 2). Compared to individual CENP-A nucleosomes, these complexes were substantially larger. Notably, these structures were not observed in either control mock IPs, bulk chromatin, or CENP-A N-ChIP (Figures 4A, B, S6), suggesting these structures arise from CENP-C/CCAN bound complex. Interestingly, by AFM, we observed that the largest of CENP-C complexes tends to be associated with a ~230bp long nucleosome-free DNA (Figure 4A, Table S4, Raw Data File 2). The same samples, analyzed in parallel by TEM, displayed similar features (Figure 4B), including the association of four to six nucleosomes at the periphery of the complex.

We next turned our attention to individual nucleosomes associated with the CENP-C complex. In our previous work, *in vitro* reconstituted recombinant octameric CENP-A nucleosomes on 601 or α-satellite DNA behave similar to H3 when measured by in-air AFM, with average heights of ~2.4 nm and widths of ~12 nm (Walkiewicz *et al.*, 2014b; Athwal *et al.*, 2015). This observation is consistent with static measurements made by biophysical, EM, and crystallographic methods, which generally show that except for flexible exit/entry DNA termini and loop 1, *in vitro* reconstituted CENP-A nucleosomes have dimensions similar to H3 nucleosomes (Tachiwana *et al.*, 2011; Walkiewicz *et al.*, 2014b; Kim *et al.*, 2016; Roulland *et al.*, 2016; Vlijm *et al.*, 2017).

In contrast, native CENP-A nucleosomes purified from either fruit fly or human cell lines generally display smaller dimensions compared to native H3 nucleosomes, except during S phase

(Dalal *et al.*, 2007; Dimitriadis *et al.*, 2010; Bui *et al.*, 2012, 2013; Athwal *et al.*, 2015). Indeed, we recapitulated these observations here. Relative to H3 nucleosomes (2.5±0.3 nm) (Figure 4C, Table S5, Raw Data File 3), native bulk CENP-A nucleosomes not associated with CENP-C are continue to be uniquely identifiable by their smaller average height of 1.9±0.3 nm (Figure 4C).

We next examined CENP-A nucleosomes that are physically associated with the CENP-C complexes (Figure 4C, Table S5, Raw Data File 3). To our surprise, these nucleosomes had distinctly larger dimensions, with a height of 2.4±0.5 nm (Figure 4C), significantly taller than bulk CENP-A nucleosomes alone (two-sided t-test $p < 0.001$).

These results point to the presence of two physically distinct CENP-A nucleosomes within the human centromere: one species of CENP-A nucleosome which is shorter, and another species of CENP-A nucleosome associated with the CENP-C/CCAN complex (Figure 4D), which adopts a taller configuration.

CENP-C overexpression does not lead to increased DNA breaks

Cumulatively, the data above suggest that one type of structure in the inner kinetochore is comprised of a polygonal dome-like structure with a roughly circular footprint, associated with a chromatin sub-domain comprised of four to six octameric CENP-A nucleosomes. Yet another type of domain in the centromere contains smaller CENP-A nucleosomes. Chromatin fiber studies show that CENP-A and H3 chromatin domains are interspersed (Blower *et al.*, 2002; Sullivan and Karpen, 2004; Ribeiro *et al.*, 2010; Kyriacou and Heun, 2018). Indeed, recent work show that CENP-C and CENP-A do not perfectly overlap on chromatin fibers (Padeganeh *et al.*,

2013; Kyriacou and Heun, 2018). Recent structural studies of CENP-A nucleosome suggest that CENP-A nucleosome are innately flexible compared to H3 nucleosomes (Winogradoff *et al.*, 2015; Falk *et al.*, 2016; Roulland *et al.*, 2016; Malik *et al.*, 2018; Melters *et al.*, 2019), whereas CENP-C suppresses CENP-A nucleosomes motions (Falk *et al.*, 2015, 2016; Melters *et al.*, 201 9 biorxiv). This raises an intriguing question on potential roles for maintaining unbound or free CENP-A centromeric chromatin *in vivo*.

We hypothesized that during mitosis flexible CENP-A particles might provide a mechanical "bungee"-like state, which allows the dissipation of mitotic forces. In this scenario, excess CENP-C would dampen the motions of CENP-A nucleosomes, thereby reducing the overall springiness of centromeric chromatin; and loss of the flexible CENP-A domain might result in an accumulation of DNA breaks during mitosis. To test this hypothesis, we overexpressed C-terminally tagged GFP CENP-C (CENP-C^{OE}) for three days, in cells synchronized to late mitosis and early G1 and scored for the DNA break marker γH2A.X. Although we found an increase in mitotic defects, no appreciable increase in γH2A.X foci was observed at centromeric foci (Figure 5). These data suggest that partial reduction in the amount of free CENP-A does not cause an increase in DNA breaks during mitosis, although it does correlate with mitotic defects.

CENP-C overexpression limits *de novo* CENP-A loading

Next, we hypothesized that free CENP-A chromatin might be necessary for centromeric transcription. RNAP2 mediated centromeric transcription has been shown to be critical for *de novo* CENP-A loading (reviewed in Müller and Almouzni, 2017) in multiple species. In parallel work, we have observed that overexpression of CENP-C results in reduced RNAP2 levels at

centromeric chromatin (Melters *et al.*, 2019). Therefore, a logical prediction is that limiting access of the transcriptional machinery to CENP-A chromatin (Figures 6A, B), should reduce new CENP-A loading. An initial clue supporting this possibility was deduced from western blot analysis, in which over-expression of CENP-C led to a significant reduction in the free CENP-A population (two-sided t-test $p<0.05$; Figure 6B, Table S6). To test whether CENP-C^{OE} would specifically lead to a reduction in new CENP-A loading, we turned to the well-established SNAP-tagged CENP-A system combined with quench pulse-chase immunofluorescence (Bodor *et al.*, 2012). Using this system in cells synchronized to mid-G1, one can distinguish between older CENP-A (TMR-block) and newly incorporated CENP-A (TMR-Star) (Figures 6C, D). Strikingly, in the CENP-C overexpression background, in which we observed RNAP2 is depleted from centromeric chromatin in early G1 (Figure 6A, B), we concomitantly observed a 2.3-fold reduction of *de novo* incorporation of CENP-A (two-sided t-test $p<0.00001$; Figures 6E, F, Raw Data File 4). Therefore, *in vivo* CENP-C^{OE} leads to suppression of RNAP2 occupancy, reduction in total free CENP-A levels (Figures 6A, B), and a reduction in *de novo* CENP-A loading (Figures 6E, F).

CENP-A mutants rescue mitotic defects caused by CENP-C overexpression

As has been reported previously in chicken DT-40 cells (Fukagawa *et al.*, 1999), we observed that overexpressing CENP-C resulted in a quantifiable increase in mitotic defects (40% normal, 60% abnormal) relative to wildtype cells (74% normal, 36% abnormal), most notably lagging chromosomes and multipolar spindles (Figure 7A, B).

CENP-C functionally docks at C-terminal tail of CENP-A nucleosomes (Carroll *et al.*, 2010; Kato *et al.*, 2013; Falk *et al.*, 2015, 2016; Guo *et al.*, 2017). We reasoned that expressing CENP-A mutants which can either sequester away excess CENP-C, or which are insensitive to CENP-C, should rescue the defects noted above. Therefore, in the background of CENP-C over-expression, we expressed either a fusion of H3 with the C-terminal tail of CENP-A ($H3^{CpA\ CTD}$) which can bind CENP-C, or CENP-A lacking its C-terminal tail ($CENP\text{-}A^{\Delta CTD}$) which can still be deposited to centromeres by the chaperone HJURP, but which cannot bind CENP-C (Figure 7A).

In the background of CENP-C overexpression, $H3^{CpA\ CTD}$ should function as a sink for excess CENP-C. In contrast, $CENP\text{-}A^{\Delta CTD}$ should reintroduce a free CENP-A population. Indeed, upon scoring mitotic cells in the background of overexpressing CENP-C and the two mutants, we observed that multipolar spindle defects were rescued by both $H3^{CpA\ CTD}$ (58% normal, 42% abnormal), or $CENP\text{-}A^{\Delta CTD}$ (65% normal, 35% abnormal) (Figure 7B).

Together, these data suggest that in the CENP-C overexpression background, there is depletion of RNAP2 at the centromeric chromatin and free CENP-A levels (Figures 6A, B), reduced incorporation of *de novo* CENP-A (Figure 6E, F), and an increase in mitotic defects (Figure 7B). Reintroducing either a free CENP-A population or $H3^{CpA\ CTD}$ sink results in a rescue of mitotic defects (Figure 7B). These data implicate a model where a balance between kinetochore bound and free CENP-A chromatin is important for proper centromere integrity.

Discussion

Since the discovery of CENP-A (Earnshaw and Rothfield, 1985; Palmer *et al.*, 1991), it has been demonstrated that CENP-A nucleosomes are required and sufficient to form kinetochores (Regnier *et al.*, 2005; Mendiburo *et al.*, 2011). At the same time, it is puzzling that more CENP-A nucleosomes reside at the centromere than are strictly needed to successfully seed a kinetochore (Bodor *et al.*, 2013; McKinley and Cheeseman, 2016). Indeed, while our study was in review and revision, a recent chromatin fiber study employed a proximity based labeling technique, finding that not all CENP-A foci colocalize with CENP-C foci (Kyriacou and Heun, 2018). Our data supports, and extends this finding. We report on the existence of two classes CENP-A nucleosomes *in vivo*. One class of CENP-A nucleosomes was strongly associated with the CENP-C complex, along with other components of the inner kinetochore/CCAN; whereas another population of CENP-A nucleosomes is weakly associated with CENP-C. Strikingly CENP-A nucleosomes associated with the CENP-C complex have altered dimensions relative to bulk CENP-A nucleosomes alone (Figure 4D). All atom computational modeling has previously indicated that CENP-A nucleosomes have a weaker four helix bundle resulting in an intrinsically more disordered nucleosome core compared to a canonical H3 nucleosome (Winogradoff *et al.*, 2015), that this flexibility arises from the CENP-A/H4 dimer (Zhao *et al.*, 2016), is lost in the tetramer (Zhao *et al.*, 2019) but regained in the CENP-A octamer upon binding of H2A and H2B, resulting in an energetically "frustated" nucleosome, which predicts the existence of multiple deformation states of CENP-A (Winogradoff *et al.*, 2015; Bui *et al.,* 2012). These data also predict that kinetochore components especially CENP-C could fix one preferred conformational state. Indeed, previous *in vitro* work has shown that both the central domain and the conserved CENP-C motif make contact with the CENP-A C-terminal tail and H2A acidic patch (Kato *et al.*, 2013). In hydrogen-deuterium exchange and smFRET experiments of *in vitro*

reconstituted CENP-A mononucleosomes, these contacts result in changes in the overall shape of CENP-A nucleosome by bringing the two nucleosome halves closer together and limiting the DNA sliding (Falk *et al.*, 2015, 2016; Guo *et al.*, 2017). As a result, the CENP-A nucleosome when bound to the central domain of CENP-C has an appearance similar to a canonical H3 nucleosome. Indeed, we observe a shift in nucleosomal height when CENP-A nucleosomes associate with CENP-C complexes. We interpret this shift to mean that the CENP-C complex stabilizes the octameric conformation of the CENP-A nucleosome *in vivo*. We do not exclude that other factors which may cause the nucleosomal height to increase, such as the binding of a non-histone CCAN partner, are equally plausible.

Interestingly, overexpression of CENP-C in HeLa cells induced a 6-fold increase in multipolar spindles and 2-fold increase in lagging chromosome (Figure 7). A correlation between multipolar spindles and merotelic chromosome attachment was described (Silkworth *et al.*, 2009). Merotelic attachment are a common feature of cancer cells and are believed to be a driving force of chromosome instability (CIN) (Salmon *et al.*, 2005; Gregan *et al.*, 2011). Interestingly, both the multipolar and the lagging chromosome phenotype we observed were rescued by re-establishing a balance between the two CENP-A domains (Figure 7). This raises the possibility that multipolar spindles can be directly regulated by either the kinetochore or possibly even CENP-C. Several important questions arise from this observation; first, does overexpression of CENP-C create a platform which might allow a larger kinetochore to be formed, thereby promoting merotelic attachments; second, does free CENP-A chromatin provide cues to direct the kinetochore to face the spindle poles, either by organizing centromeric chromatin and/or by

regulating inner centromere proteins localization, like Aurora B? These will be interesting questions to pursue in follow-up work.

In addition, overexpression of CENP-C also reduced the level of *de novo* incorporation of CENP-A nucleosomes (Figure 6E, F). Previous work has shown that CENP-A incorporation is dependent on centromeric transcription (reviewed in Müller and Almouzni, 2017). Indeed, levels of centromeric RNAP2 were reduced in early G1 (Figure 6B), providing further evidence that nucleosome loading requires polymerase activity. Furthermore, recent work showed that CENP-C has the capacity to limit CENP-A nucleosome's innate motions (Falk *et al.*, 2015, 2016), as well as compact CENP-A chromatin (Melters *et al.*, 2019). Altogether, this points to the intriguing possibility that CENP-C overexpression alters centromeric chromatin is such a way that it becomes less accessible to various factors, including the transcriptional machinery. This in juxtaposition to free or unbound CENP-A chromatin, which is unable to bind to H1 (Roulland *et al.*, 2016) and has extensive linker DNAs (Dalal *et al.*, 2007), combined with the intrinsic distortability might (Henikoff and Dalal, 2005; Winogradoff *et al.*, 2015; Malik *et al.*, 2018) create an innate open chromatin state, readily accessible to various factors, including the transcriptional machinery. Nevertheless, in wild-type condition we observed RNAP2 to be present in both CENP-A populations. This raises the question, if CENP-C associated CENP-A chromatin is less accessible, how did RNAP2 get there? One interesting possibility is that the entry and exit DNA strands of CENP-C associated CENP-A nucleosomes are as accessible as unbound CENP-A nucleosomes, but access to the DNA wrapped by the CENP-A nucleosome is impaired upon CENP-C binding. To load RNAP2 to the chromatin fiber, the pre-initiation complex has to be formed first. Thus, it will be interesting to learn if the pre-initiation complex

forms at the free CENP-A chromatin, or on the bordering H3K4Me3 containing domains mapped withih the centromere (Blower *et al.*, 2002; Sullivan and Karpen, 2004).

In summary, in this report we describe that CENP-A nucleosomes display two alternative conformational states *in vivo,* both of which are important for centromere fidelity in cycling cells. Nucleosome dynamics play an important role in genome compaction, protection from DNA damaging agents, and regulating DNA access by DNA binding factors. These dynamics are driven by only a few interactions between the interfaces of DNA and nucleosomes (Polach and Widom, 1995; Widom, 2002; Fierz and Poirier, 2019). Recently, we described a CENP-A core post-translation modification (PTM) that altered the binding of CENP-C to CENP-A *in vivo* (Bui *et al.*, 2017). An exciting line of future investigation is to examine how DNA or histone modifications which promote specific conformations of CENP-A nucleosomes, might alter its interactions with chaperones, kinetochore partners, and its occupancy on centromere α-satellite DNA. It will also be of \interest to investigate whether nucleosome stabilizing or destabilizing interactions promote or suppress centromeric transcription required for the epigenetic memory of centromeres in various species (Wong *et al.*, 2007; Li *et al.*, 2008; Chueh *et al.*, 2009; Ferri *et al.*, 2009; Bergmann *et al.*, 2011; Ohkuni and Kitagawa, 2011; Choi *et al.*, 2011; Lyn Chan and Wong, 2012; Quénet and Dalal, 2014; Rošić *et al.*, 2014; Catania *et al.*, 2015; Grenfell *et al.*, 2016; McNulty *et al.*, 2017; Bobkov *et al.*, 2018; Zhu *et al.*, 2018; Melters *et al.*, 2019; Ling and Yuen, 2019), and for chaperone interactions required for correct targeting of CENP-A, which we, and others, have demonstrated is defective in cancer cells (Athwal *et al.*, 2015; Zhao *et al.*, 2016; Nye *et al.*, 2018).

Material and Methods

Key Resources Table

Reagents or Resource	Source	Identifier	Application	Quantity
ACA serum	BBI Solutions	SG140-2	N-ChIP, X-ChIP	5 µL
Anti-CENP-A (rabbit)	Custom made		N-ChIP	3 µL
Anti-CENP-A (mouse)	Abcam	ab13939	IF	1:1000
Anti-CENP-A (rabbit)	Abcam	ab45694	WB	1:3000
Anti-CENP-A (rabbit)	Milipore	04-205	WB	1:3000
Anti-CENP-B (rabbit)	Santa Cruz	sc-22788	WB	1:500
Anti-CENP-C (guinea pig)	MBL International	PD030	N-ChIP, X-ChIP, IF	5 µL, 1:1000
Anti-CENP-C (rabbit)	Santa Cruz	sc-22789	WB	1:500
Anti-CENP-N	Avivasysbio	ARP57258-P050	WB	1:500
Anti-CENP-I	Bethyl	A303-374A	WB	1:1000
Anti-CENP-T	Bethyl	A302-314A	WB	1:1000
Anti-CENP-W	Invitrogen	PA5-34441	WB	1:300
Anti-MIS12	Abcam	ab70843	WB	1:500
Anti-HEC1/NDC80	GeneTex	GTX70268	WB	1:1000
Anti-macroH2A.1	Abcam	ab37264	WB	1:1000
Anti-γH2A.X	Abcam	ab11174	IF	1:1000
Anti-γH2A.X	Abcam	ab2893	WB	1:1000
Anti-H2A.Z	Abcam	ab4179	WB	1:1000
Anti-H2A	Abcam	ab18255	WB	1:1000
Anti-H2B	Abcam	ab1790	WB	1:1000
Anti-H4	Cell Signaling	2935T	WB	1:1000
Anti-H3	Santa Cruz	sc-8654	WB	1:3000

Software and Algorithms		
Software and Algorithms		
RepBase		hhtp://www.girinst.org/repbase
Gwyddion		http://gwyddion.net/
R		https://www.r-project.org/
NIH ImageJ		https://imagej.nih.gov/ij/
Bio-Formats		https://www.openmicroscopy.org/bio-formats/
CRaQ		http://facilities.igc.gulbenkian.pt/microscopy/microscopy-macros.php

Native and cross-linked Chromatin-Immunoprecipitation and Western blotting

Human cell line HeLa were grown in DMEM (Invitrogen/ThermoFisher Cat #11965) supplemented with 10% FBS and 1X penicillin and streptomycin cocktail. N-ChIP experiments were performed without fixation. After cells were grown to ~80% confluency, they were harvested as described (Bui *et al.*, 2012, 2017). For best results for chromatin preparation for

AFM the pellet that is obtained after each spin-down during the nuclei extraction protocol (Walkiewicz *et al.*, 2014a) is broken up with a single gentle tap. Nuclei were digested for 6 minutes with 0.25 U MNase/mL (Sigma-Aldrich cat #N3755-500UN) and supplemented with 1.5 mM $CaCl_2$. Following quenching (10 mM EGTA), nuclei pellets were spun down, and chromatin was extracted gently, overnight in an end-over-end rotator, in low salt solution (0.5X PBS; 0.1 mM EGTA; protease inhibitor cocktail (Roche cat #05056489001). N-ChIP chromatin bound to Protein G Sepharose beads (GE Healthcare cat #17-0618-02) were gently washed twice with ice cold 0.5X PBS and spun down for 1 minute at 4ºC at 800 rpm. Following the first N-ChIP, the unbound fraction was used for the sequential N-ChIP. X-ChIP experiments were performed with fixation (Skene and Henikoff, 2015). Westerns analyses were done using LiCor's Odyssey CLx scanner and Image Studio v2.0.

Glycerol gradient sedimentation

A total of 2 mL of extracted chromatin was applied to 10 mL of 5 to 20% glycerol gradient containing 50 mM Tris-HCl pH 8.0, 2 mM EDTA, 0.1% NP-40, 2 mM DTT, 0.15 M NaCl, and 1X protease inhibitor cocktail layered over 0.4 mL of 50% glycerol. The chromatin was centrifuged with a SW41Ti rotor (Beckman) at 22,000 rpm for 15.5 hours at 4ºC. 1 mL aliquots were fractioned from the top, and DNA and protein samples were separated by either 1.2% agarose gel electrophoreses or 4-20% SDS-PAGE gels, respectively. Serial N-ChIP was performed on all 12 fractions.

AFM and image analysis

Imaging of CENP-C and CENP-A N-ChIP and bulk chromatin was performed as described (Dimitriadis *et al.*, 2010; Walkiewicz *et al.*, 2014a) with the following modifications. Imaging was performed by using standard AFM equipment (Oxford Instruments, Asylum Research's Cypher S AFM, Santa Barbara, CA) with silicon cantilevers (OTESPA or OTESPA-R3 with nominal resonances of ~300 kHz, stiffness of ~42 N/m, and tip radii of 3–7 nm) in noncontact tapping mode. 10 µl of bulk , CENP-A, or CENP-C chromatin sample was deposited on APS-treated mica (Dimitriadis *et al.*, 2010; Walkiewicz *et al.*, 2014a). The samples were incubated for 10 min, rinsed gently to remove salts, and dried mildly under vacuum before imaging. Automated image analysis was performed as described in (Walkiewicz *et al.*, 2014a) with the only modifications that R software was used instead of Microsoft Excel. A total of six biological replicates were performed for CENP-C experiments and three biological replicates for both the CENP-A and bulk chromatin experiments. Bulk chromatin from the same preparation was imaged in parallel to get the baseline octameric range. For all samples, manual spot analyses were performed to confirm accuracy of automated analyses.

Immuno-AFM

In vitro reconstitution of CENP-A (CENP-A/H4 cat#16-010 and H2A/H2B cat#15-0311, EpiCypher, Research Triangle Park, NC) and H3 (H3/H4 cat#16-0008 and H2A/H2B cat#15-0311, EpiCypher Research Triangle Park, NC) nucleosomes were performed as previously described (Dimitriadis *et al.*, 2010; Walkiewicz *et al.*, 2014a). Chromatin from HeLa cells were obtained from fractions 6 and 7 of a glycerol density gradient (containing on average tri-, tetra-, and penta-nucleosome arrays). These samples were subjected to immuno-AFM as described previously (M. E. Browning-Kelley *et al.*, 1997; Cheung and Walker, 2008; Banerjee *et al.*,

2012). An aliquot of each sample was imaged by AFM in non-contact tapping mode. The remainder of the samples were incubated overnight at 4ºC with anti-CENP-A antibody (Abcam cat #ab13939) in an end-over-end rotator before being imaged by AFM. Finally, these samples were incubated with anti-mouse secondary antibody (Li-Cor's IRDye 800CW Donkey anti-mouse IgG cat#925-32212) for an hour at room-temperature in an end-over-end rotator and imaged by AFM in non-contact tapping mode. We analyzed the height profiles of the nucleosomes and antibody complexes as described above.

Transmission electron microscopy

For transmission electron microscopy (TEM), the N-ChIP samples were fixed by adding 0.1% glutaraldehyde at 4ºC for 5 hours, followed by 12-hour dialysis against HNE buffer (10 mM HEPES pH=7.0, 5 mM NaCl, 0.1 mM EDTA) in 20,000 MWCO membranes dialysis cassettes (Slide-A-Lyzer Dialysis Cassette, ThermoFisher cat #66005) at 4ºC. The dialyzed samples were diluted to about 1 µg/mL concentration with 67.5 mM NaCl, applied to carbon-coated and glow-discharged EM grids (T1000-Cu, Electron Microscopy Sciences), and stained with 0.04% uranyl acetate. Dark-field EM imaging was conducted at 120 kV using JEM-1000 electron microscope (JEOL USA, Peabody, MA) with SC1000 ORIUS 11 megapixel CCD camera (Gatan, Inc. Warrendale, PA).

Immunostaining of mitotic chromosomes

HeLa cells were synchronized to mitosis with double thymidine block. Primary antibodies γH2A.X, CENP-C, and CENP-A were used at dilution 1:1000. Alexa secondary (488, 568, 647) were used at dilution of 1:1000. Images were obtained using DeltaVision RT system fitted with a

CoolSnap charged-coupled device camera and mounted on an Olympus IX70. Deconvolved IF images were processed using ImageJ. Mitotic defects (lagging chromosomes and/or multipolar spindles) were counted for 83 and 76 cells (mock, GFP-CENP-C, respectively).

Quench pulse-chase immunofluorescence

To quantify *de novo* assembled CENP-A particles, we transfected HeLa cells with SNAP-tagged CENP-A (generous gift from Dan Foltz) in combination with either empty vector or GFP-CENP-C using the Amaxa Nucleofector kit R (Lonza Bioscience, Walkersville, MD) per instructions. The quench pulse-chase experiment was performed according to Bodor et al[17]. In short, following transfection, cells were synchronized with double thymidine block. At the first release TMR-block (S9106S, New England Biolabs, Ipswich, MA) was added per manufactures instruction and incubated for 30 min at 37ºC, followed by three washes with cell culture media. At the second release TMR-Star (S9105S, New England Biolabs, Ipswich, MA) was added per manufactures instructions and incubated for 15 min at 37ºC, followed by three washes with cell culture media. Fourteen hours after adding TMR-Star, cells were fixed with 1% paraformaldehyde in PEM (80 mM K-PIPES pH 6.8, 5 mM EGTA pH 7.0, 2 mM $MgCl_2$) for 10 min at RT. Next, cells were washed the cells three times with ice cold PEM. To extract soluble proteins, cells were incubated with 0.5% Triton-X in CSK (10 mM K-PIPES pH 6.8, 100 mM NaCl, 300 mM sucrose, 3 mM $MgCl_2$, 1 mM EGTA) for 5 min at 4ºC. The cells were rinsed with PEM and fixed for a second time with 4% PFA in PEM for 20 min at 4ºC. Next, the cells were washed three times with PEM. Cells were permeabilized with 0.5% Triton-X in PEM for 5 min at RT and subsequently washes three times with PEM. Next, the cells were incubated in blocking solution (1X PBS, 3% BSA, 5% normal goat serum) for 1 hr at 4ºC. CENP-A antibody (ab13979

1:1000) was added for 1 hr at 4ºC, followed by three washes with 1X PBS-T. Anti-mouse secondary (Alexa-488 1:1000) was added for 1hr at 4ºC, followed by three 1X PBS-T and two 1X PBS washes. Following air-drying, cells were mounted with Vectashield with DAPI (H-1200, Vector Laboratories, Burlingame, CA) and the coverslips were sealed with nail polish. Images were collected using a DeltaVision RT system fitted with a CoolSnap charged-coupled device camera and mounted on an Olympus IX70. Deconvolved IF images were processed using ImageJ. From up to 22 nuclei, colocalizing CENP-A and TMR-Star foci signal were collected, as well directly neighboring regions. Background signal intensity was deducted from corresponding CENP-A and TMR-Star signal intensity before the ratio CENP-A/TMR-Star was determined. Graphs were prepared using the ggplot2 package for R.

ChIP-seq

CENP-C N-ChIP followed by ACA N-ChIP was conducted, as well as an IgG N-ChIP and input control as described above. Next, DNA was isolated by first proteinase K treated the samples, followed by DNA extraction by phenol chloroform. The samples were used to prepare libraries for PacBio single-molecule sequencing as described in manufacturer's protocol (PacBio, Menlo Park, CA). Libraries were produced and loaded on ZWM chip either by diffusion or following size selection of the inserts (> 1000 bp) for all four samples. Subsequently, the reads were sequenced on the PacBio RS II operated by Advanced Technology Center, NCI (Frederick, MD). Sequence reads were mapped to either sequences in RepBase, the consensus sequence used by (Hasson *et al.*, 2013), and the consensus sequences used by (Henikoff *et al.*, 2015). The sequence data can be found under GEO accession number GSE129351.

Quantification and statistical analyses

Significant differences for Western blot quantification and nucleosome height measurements from AFM analyses were performed using either paired or two-sided t-test as described in the figure legends. Significance was determined at $p<0.05$.

Footnotes

Authors contributions: D.P.M., T.R., and Y.D. designed research; D.P.M., T.R, B.M., S.A.G., and D.S. performed research; D.P.M., T.R., B.M., S.A.G., D.S., and Y.D. analyzed data; D.P.M. prepared figures; and D.P.M. and Y.D. wrote the paper; all authors editing the paper.

The authors declare no conflict of interest.

Acknowledgements

We thank Drs. Tom Misteli and Sam John, and members of the CSEM laboratory for critical comments and suggestions. We thank Dr. Kerry Bloom for encouraging us to purify kinetochore bound CENP-A. We thank Dr. Andrea Musacchio for comments on a previous version of this manuscript. We thank Drs. Heinz and Dimitriadis for technical assistance on the AFM. This work utilized the computational resources of the NIH HPC Biowulf cluster (http://hpc.nih.gov). Y.D. and T.R, B.M., D.S., and D.P.M. were supported by the Intramural Research Program of the Center for Cancer Research at the National Cancer Institute/NIH. S.A.G. was supported by NSF grant 1516999.

References

Athwal, RK, Walkiewicz, MP, Baek, S, Fu, S, Bui, M, Camps, J, Ried, T, Sung, MH, and Dalal, Y (2015). CENP-A nucleosomes localize to transcription factor hotspots and subtelomeric sites in human cancer cells. Epigenetics and Chromatin.

Bailey, AO, Panchenko, T, Shabanowitz, J, Lehman, SM, Bai, DL, Hunt, DF, Black, BE, and Foltz, DR (2016). Identification of the Post-translational Modifications Present in Centromeric Chromatin. Mol Cell Proteomics.

Banerjee, S, M, A, Rakshit, T, Roy, NS, Kundu, TK, Roy, S, and Mukhopadhyay, R (2012). Structural features of human histone acetyltransferase p300 and its complex with p53. FEBS Lett 586, 3793–3798.

Bergmann, JH, Rodríguez, MG, Martins, NMC, Kimura, H, Kelly, DA, Masumoto, H, Larionov, V, Jansen, LET, and Earnshaw, WC (2011). Epigenetic engineering shows H3K4me2 is required for HJURP targeting and CENP-A assembly on a synthetic human kinetochore. EMBO J.

Bloom, KS, and Carbon, J (1982). Yeast centromere DNA is in a unique and highly ordered structure in chromosomes and small circular minichromosomes. Cell.

Blower, MD, Sullivan, BA, and Karpen, GH (2002). Conserved organization of centromeric chromatin in flies and humans. Dev Cell 2, 319–330.

Bobkov, GOM, Gilbert, N, and Heun, P (2018). Centromere transcription allows CENP-A to transit from chromatin association to stable incorporation. J Cell Biol.

Bodor, DL, Mata, JF, Sergeev, M, David, AF, Salimian, KJ, Panchenko, T, Cleveland, DW, Black, BE, Shah, J V, and Jansen, LE (2014). The quantitative architecture of centromeric chromatin. Elife.

Bodor, DL, Rodríguez, MG, Moreno, N, and Jansen, LET (2012). Analysis of protein turnover by quantitative SNAP-based pulse-chase imaging. Curr Protoc Cell Biol.

Bodor, DL, Valente, LP, Mata, JF, Black, BE, and Jansen, LET (2013). Assembly in G1 phase and long-term stability are unique intrinsic features of CENP-A nucleosomes. Mol Biol Cell.

Bui, M, Dimitriadis, EK, Hoischen, C, An, E, Quénet, D, Giebe, S, Nita-Lazar, A, Diekmann, S, and Dalal, Y (2012). Cell-cycle-dependent structural transitions in the human CENP-A nucleosome in vivo. Cell.

Bui, M, Pitman, M, Nuccio, A, Roque, S, Donlin-Asp, PG, Nita-Lazar, A, Papoian, GA, and Dalal, Y (2017). Internal modifications in the CENP-A nucleosome modulate centromeric dynamics. Epigenetics and Chromatin.

Bui, M, Walkiewicz, MP, Dimitriadis, EK, and Dalal, Y (2013). The CENP-A nucleosome. A battle between Dr. Jekyll and Mr. Hyde. Nucl (United States).

Carroll, CW, Milks, KJ, and Straight, AF (2010). Dual recognition of CENP-A nucleosomes is required for centromere assembly. J Cell Biol.

Catania, S, Pidoux, AL, and Allshire, RC (2015). Sequence Features and Transcriptional Stalling within Centromere DNA Promote Establishment of CENP-A Chromatin. PLoS Genet.

Cheeseman, IM (2014). The Kinetochore. Cold Spring Harb Perspect Biol 6, a015826–a015826.

Cheeseman, IM, Chappie, JS, Wilson-Kubalek, EM, and Desai, A (2006). The Conserved KMN Network Constitutes the Core Microtubule-Binding Site of the Kinetochore. Cell.

Cheung, JWC, and Walker, GC (2008). Immuno-Atomic Force Microscopy Characterization of Adsorbed Fibronectin. Langmuir 24, 13842–13849.

Choi, ES, Strålfors, A, Castillo, AG, Durand-Dubief, M, Ekwall, K, and Allshire, RC (2011). Identification of noncoding transcripts from within CENP-A chromatin at fission yeast centromeres. J Biol Chem.

Chueh, AC, Northrop, EL, Brettingham-moore, KH, Choo, KHA, and Wong, LH (2009). LINE

Retrotransposon RNA Is an Essential Structural and Functional Epigenetic Component of a Core Neocentromeric Chromatin. PLoS Genet 5.

Comings, DE, and Okada, TA (1970). Whole-mount electron microscopy of the centromere region of metacentric and telocentric mammalian chromosomes. Cytogenetics 9, 436–449.

Cooper, JL, and Henikoff, S (2004). Adaptive evolution of the histone fold domain in centromeric histones. Mol Biol Evol 21, 1712–1718.

Dalal, Y, Wang, H, Lindsay, S, and Henikoff, S (2007). Tetrameric structure of centromeric nucleosomes in interphase Drosophila cells. PLoS Biol 5 E218.

DeLuca, JG, and Musacchio, A (2012). Structural organization of the kinetochore-microtubule interface. Curr Opin Cell Biol.

Díaz-Ingelmo, O, Martínez-García, B, Segura, J, Valdés, A, and Roca, J (2015). DNA Topology and Global Architecture of Point Centromeres. Cell Rep.

Dimitriadis, EK, Weber, C, Gill, RK, Diekmann, S, and Dalal, Y (2010). Tetrameric organization of vertebrate centromeric nucleosomes. Proc Natl Acad Sci.

Earnshaw, WC, and Rothfield, N (1985). Identification of a family of human centromere proteins using autoimmune sera from patients with scleroderma. Chromosoma.

Esponda, P (1978). Cytochemistry of kinetochores under electron microscopy. Exp Cell Res 114, 247–252.

Falk, SJ et al. (2015). CENP-C reshapes and stabilizes CENP-A nucleosomes at the centromere. Science (80-).

Falk, SJ, Lee, J, Sekulic, N, Sennett, MA, Lee, TH, and Black, BE (2016). CENP-C directs a structural transition of CENP-A nucleosomes mainly through sliding of DNA gyres. Nat Struct Mol Biol.

Ferri, F, Bouzinba-Segard, H, Velasco, G, Hubé, F, and Francastel, C (2009). Non-coding murine centromeric transcripts associate with and potentiate Aurora B kinase. Nucleic Acids Res.

Fierz, B, and Poirier, MG (2019). Biophysics of Chromatin Dynamics. Annu Rev Biophys.

Foltz, DR, Jansen, LET, Black, BE, Bailey, AO, Yates, JR, and Clevel, DW (2006). The human CENP-A centromeric nucleosome-associated complex. Nat Cell Biol 8, 458–469.

Fukagawa, T, Pendon, C, Morris, J, and Brown, W (1999). CENP-C is necessary but not sufficient to induce formation of a functional centromere. EMBO J.

Furuyama, T, Codomo, CA, and Henikoff, S (2013). Reconstitution of hemisomes on budding yeast centromeric DNA. Nucleic Acids Res.

Furuyama, T, and Henikoff, S (2009). Centromeric nucleosomes induce positive supercoils. Cell 138, 104–113.

Gonen, S, Akiyoshi, B, Iadanza, MG, Shi, D, Duggan, N, Biggins, S, and Gonen, T (2012). The structure of purified kinetochores reveals multiple microtubule-attachment sites. Nat Struct Mol Biol.

Gregan, J, Polakova, S, Zhang, L, Tolić-Nørrelykke, IM, and Cimini, D (2011). Merotelic kinetochore attachment: Causes and effects. Trends Cell Biol.

Grenfell, AW, Heald, R, and Strzelecka, M (2016). Mitotic noncoding RNA processing promotes kinetochore and spindle assembly in Xenopus. J Cell Biol.

Guo, LY et al. (2017). Centromeres are maintained by fastening CENP-A to DNA and directing an arginine anchor-dependent nucleosome transition. Nat Commun.

Hasson, D, Panchenko, T, Salimian, KJ, Salman, MU, Sekulic, N, Alonso, A, Warburton, PE, and Black, BE (2013). The octamer is the major form of CENP-A nucleosomes at human

centromeres. Nat Struct Mol Biol.

Henikoff, JG, Thakur, J, Kasinathan, S, and Henikoff, S (2015). A unique chromatin complex occupies young a-satellite arrays of human centromeres. Sci Adv.

Henikoff, S, Ahmad, K, and Malik, HS (2001). The centromere paradox: Stable inheritance with rapidly evolving DNA. Science (80-).

Henikoff, S, and Dalal, Y (2005). Centromeric chromatin: What makes it unique. Curr Opin Genet Dev 15, 177–184.

Henikoff, S, Ramachandran, S, Krassovsky, K, Bryson, TD, Codomo, CA, Brogaard, K, Widom, J, Wang, J-P, and Henikoff, JG (2014). The budding yeast Centromere DNA Element II wraps a stable Cse4 hemisome in either orientation in vivo. Elife.

Howman, E V, Fowler, KJ, Newson, AJ, Redward, S, Macdonald, AC, Kalitsis, P, and Choo, KHA (1999). Early disruption of centromeric chromatin organization in centromere protein A (Cenpa) null mice. Cycle.

Kalitsis, P, Fowler, KJ, Earle, E, Hill, J, and Choo, KHA (2002). Targeted disruption of mouse centromere protein C gene leads to mitotic disarray and early embryo death. Proc Natl Acad Sci.

Kato, H, Jiang, J, Zhou, BR, Rozendaal, M, Feng, H, Ghirlando, R, Xiao, TS, Straight, AF, and Bai, Y (2013). A conserved mechanism for centromeric nucleosome recognition by centromere protein CENP-C. Science (80-).

Kim, SH, Vlijm, R, Van Der Torre, J, Dalal, Y, and Dekker, C (2016). CENP-A and H3 nucleosomes display a similar stability to force-mediated disassembly. PLoS One.

Kingston, IJ, Yung, JSY, and Singleton, MR (2011). Biophysical characterization of the centromere-specific nucleosome from budding yeast. J Biol Chem.

Klare, K, Weir, JR, Basilico, F, Zimniak, T, Massimiliano, L, Ludwigs, N, Herzog, F, and

Musacchio, A (2015). CENP-C is a blueprint for constitutive centromere-associated network assembly within human kinetochores. J Cell Biol.

Krassovsky, K, Henikoff, JG, and Henikoff, S (2011). Tripartite organization of centromeric chromatin in budding yeast. Proc Natl Acad Sci.

Kwon, M-S, Hori, T, Okada, M, and Fukagawa, T (2007). CENP-C Is Involved in Chromosome Segregation, Mitotic Checkpoint Function, and Kinetochore Assembly. Mol Biol Cell.

Kyriacou, E, and Heun, P (2018). High-resolution mapping of centromeric protein association using APEX-chromatin fibers. Epigenetics Chromatin 11, 68.

Lacoste, N, Woolfe, A, Tachiwana, H, Garea, AV, Barth, T, Cantaloube, S, Kurumizaka, H, Imhof, A, and Almouzni, G (2014). Mislocalization of the Centromeric Histone Variant CenH3/CENP-A in Human Cells Depends on the Chaperone DAXX. Mol Cell.

Li, F, Sonbuchner, L, Kyes, SA, Epp, C, and Deitsch, KW (2008). Nuclear non-coding RNAs are transcribed from the centromeres of Plasmodium falciparum and are associated with centromeric chromatin. J Biol Chem.

Ling, YH, and Yuen, KWY (2019). Point centromere activity requires an optimal level of centromeric noncoding RNA. Proc Natl Acad Sci U S A.

Lyn Chan, F, and Wong, LH (2012). Transcription in the maintenance of centromere chromatin identity. Nucleic Acids Res.

M. E. Browning-Kelley, †, K. Wadu-Mesthrige, ‡, V. Hari, *,† and, and G. Y. Liu*, ‡ (1997). Atomic Force Microscopic Study of Specific Antigen/Antibody Binding.

Maheshwari, S, Tan, EH, West, A, Franklin, FCH, Comai, L, and Chan, SWL (2015). Naturally Occurring Differences in CENH3 Affect Chromosome Segregation in Zygotic Mitosis of Hybrids. PLoS Genet.

Malik, HS, and Henikoff, S (2001). Adaptive evolution of Cid, a centromere-specific histone. Dros Genet 157, 1293–1298.

Malik, HS, and Henikoff, S (2003). Phylogenomics of the nucleosome. Nat Struct Biol 10, 882–891.

Malik, N, Dantu, SC, Shukla, S, Kombrabail, M, Ghosh, SK, Krishnamoorthy, G, and Kumar, A (2018). Conformational flexibility of histone variant CENP-A Cse4 is regulated by histone H4: A mechanism to stabilize soluble Cse4. J Biol Chem.

McEwen, BF, Hsieh, CE, Mattheyses, AL, and Rieder, CL (1998). A new look at kinetochore structure in vertebrate somatic cells using high-pressure freezing and freeze substitution. Chromosoma 107, 366–375.

McKinley, KL, and Cheeseman, IM (2016). The molecular basis for centromere identity and function. Nat Rev Mol Cell Biol.

McNulty, SM, Sullivan, LL, and Sullivan, BA (2017). Human Centromeres Produce Chromosome-Specific and Array-Specific Alpha Satellite Transcripts that Are Complexed with CENP-A and CENP-C. Dev Cell.

Melters, DP et al. (2013). Comparative analysis of tandem repeats from hundreds of species reveals unique insights into centromere evolution. Genome Biol 14.

Melters, DP, Nye, J, Zhao, H, and Dalal, Y (2015). Chromatin dynamics in vivo: A game of musical chairs. Genes (Basel) 6.

Melters, DP, Pitman, M, Rakshit, T, Dimitriadis, EK, Bui, M, Papoian, GA, and Dalal, Y (2019). Intrinsic elasticity of nucleosomes is encoded by histone variants and calibrated by their binding partners. BioRxiv, 392787.

Mendiburo, MJ, Padeken, J, Fülöp, S, Schepers, A, and Heun, P (2011). Drosophila CENH3 is

sufficient for centromere formation. Science (80-).

Meraldi, P, Mcainsh, AD, Rheinbay, E, and Sorger, PK (2006). Phylogenetic and structural analysis of centromeric DNA and kinetochore proteins. Genome Biol 7, R23.

Milks, KJ, Moree, B, and Straight, AF (2009). Dissection of CENP-C-directed Centromere and Kinetochore Assembly. Mol Biol Cell.

Müller, S, and Almouzni, G (2017). Chromatin dynamics during the cell cycle at centromeres. Nat Rev Genet.

Nye, J, Sturgill, D, Athwal, R, and Dalal, Y (2018). HJURP antagonizes CENP-A mislocalization driven by the H3.3 chaperones HIRA and DAXX. PLoS One.

Ohkuni, K, and Kitagawa, K (2011). Endogenous transcription at the centromere facilitates centromere activity in budding yeast. Curr Biol.

Padeganeh, A, Ryan, J, Boisvert, J, Ladouceur, AM, Dorn, JF, and Maddox, PS (2013). Octameric CENP-A Nucleosomes Are Present at Human Centromeres throughout the Cell Cycle. Curr Biol.

Palmer, DK, O'Day, K, Trong, HL, Charbonneau, H, and Margolis, RL (1991). Purification of the centromere-specific protein CENP-A and demonstration that it is a distinctive histone. Proc Natl Acad Sci U S A.

Pesenti, ME, Weir, JR, and Musacchio, A (2016). Progress in the structural and functional characterization of kinetochores. Curr Opin Struct Biol.

Pettersen, EO, Bakke, O, Lindmo, T, and Oftebro, R (1977). CELL CYCLE CHARACTERISTICS OF SYNCHRONIZED AND ASYNCHRONOUS POPULATIONS OF HUMAN CELLS AND EFFECT OF COOLING OF SELECTED MITOTIC CELLS. Cell Prolif.

Polach, KJ, and Widom, J (1995). Mechanism of protein access to specific DNA sequences in chromatin: A dynamic equilibrium model for gene regulation. J Mol Biol.

Przewloka, MR, Zhang, W, Costa, P, Archambault, V, D'Avino, PP, Lilley, KS, Laue, ED, McAinsh, AD, and Glover, DM (2007). Molecular analysis of core kinetochore composition and assembly in Drosophila melanogaster. PLoS One.

Quénet, D, and Dalal, Y (2014). A long non-coding RNA is required for targeting centromeric protein A to the human centromere. Elife.

Rattner, JB, Branch, A, and Hamkalo, BA (1975). Electron microscopy of whole mount metaphase chromosomes. Chromosoma 52, 329–338.

Regnier, V, Vagnarelli, P, Fukagawa, T, Zerjal, T, Burns, E, Trouche, D, Earnshaw, W, and Brown, W (2005). CENP-A Is Required for Accurate Chromosome Segregation and Sustained Kinetochore Association of BubR1. Mol Cell Biol.

Remnant, L, Booth, DG, Vargiu, G, Spanos, C, Kerr, ARW, and Earnshaw, WC (2019). *In vitro* BioID: Mapping the CENP-A Micro-Environment with high temporal and spatial resolution. Mol Biol Cell, mbc.E18-12-0799.

Ribeiro, SA, Vagnarelli, P, Dong, Y, Hori, T, McEwen, BF, Fukagawa, T, Flors, C, and Earnshaw, WC (2010). A super-resolution map of the vertebrate kinetochore. Proc Natl Acad Sci.

Rošić, S, Köhler, F, and Erhardt, S (2014). Repetitive centromeric satellite RNA is essential for kinetochore formation and cell division. J Cell Biol.

Roulland, Y et al. (2016). The Flexible Ends of CENP-A Nucleosome Are Required for Mitotic Fidelity. Mol Cell.

Rudd, MK, Wray, GA, and Willard, HF (2006). The evolutionary dynamics of α -satellite The

evolutionary dynamics of ⌴ -satellite. Genome Res, 88–96.

Salmon, ED, Cimini, D, Cameron, LA, and DeLuca, JG (2005). Merotelic kinetochores in mammalian tissue cells. In: Philosophical Transactions of the Royal Society B: Biological Sciences.

Saunders, M, Fitzgerald-hayes, H, and Bloom, K (1988). Chromatin structure of altered yeast centromeres. Proc Null Acud.

Silkworth, WT, Nardi, IK, Scholl, LM, and Cimini, D (2009). Multipolar spindle pole coalescence is a major source of kinetochore mis-attachment and chromosome mis-segregation in cancer cells. PLoS One.

Skene, PJ, and Henikoff, S (2015). A simple method for generating highresolution maps of genome-wide protein binding. Elife.

Smoak, EM, Stein, P, Schultz, RM, Lampson, MA, and Black, BE (2016). Long-Term Retention of CENP-A Nucleosomes in Mammalian Oocytes Underpins Transgenerational Inheritance of Centromere Identity. Curr Biol.

Sullivan, BA, and Karpen, GH (2004). Centromeric chromatin exhibits a histone modification pattern that is distinct from both euchromatin and heterochromatin. Nat Struct Mol Biol.

Suzuki, A, Badger, BL, and Salmon, ED (2015). A quantitative description of Ndc80 complex linkage to human kinetochores. Nat Commun.

Suzuki, A, Hori, T, Nishino, T, Usukura, J, Miyagi, A, Morikawa, K, and Fukagawa, T (2011). Spindle microtubules generate tension-dependent changes in the distribution of inner kinetochore proteins. J Cell Biol.

Tachiwana, H et al. (2011). Crystal structure of the human centromeric nucleosome containing CENP-A. Nature.

Talbert, PB, Bryson, TD, and Henikoff, S (2004). of Biology BioMed Central Adaptive evolution of centromere proteins in plants and animals. J Biol.

Vargiu, G, Makarov, AA, Allan, J, Fukagawa, T, Booth, DG, and Earnshaw, WC (2017). Stepwise unfolding supports a subunit model for vertebrate kinetochores. Proc Natl Acad Sci.

Vlijm, R, Kim, SH, De Zwart, PL, Dalal, Y, and Dekker, C (2017). The supercoiling state of DNA determines the handedness of both H3 and CENP-A nucleosomes. Nanoscale.

Walkiewicz, MP, Bui, M, Quénet, D, and Dalal, Y (2014a). Tracking histone variant nucleosomes across the human cell cycle using biophysical, biochemical, and cytological analyses. Methods Mol Biol.

Walkiewicz, MP, Dimitriadis, EK, and Dalal, Y (2014b). CENP-A octamers do not confer a reduction in nucleosome height by AFM. Nat Struct Mol Biol 21, 2–3.

Wang, H, Dalal, Y, Henikoff, S, and Lindsay, S (2008). Single-epitope recognition imaging of native chromatin. Epigenetics Chromatin.

Waye, JS, and Willard, HF (2006). Human beta satellite DNA: genomic organization and sequence definition of a class of highly repetitive tandem DNA. Proc Natl Acad Sci.

Weir, JR et al. (2016). Insights from biochemical reconstitution into the architecture of human kinetochores. Nature.

Widom, J (2002). STRUCTURE, DYNAMICS, AND FUNCTION OF CHROMATIN IN VITRO. Annu Rev Biophys Biomol Struct.

Winogradoff, D, Zhao, H, Dalal, Y, and Papoian, GA (2015). Shearing of the CENP-A dimerization interface mediates plasticity in the octameric centromeric nucleosome. Sci Rep.

Wong, LH et al. (2007). Centromere RNA is a key component for the assembly of nucleoproteins at the nucleolus and centromere. Genome Res.

Zhao, H, Winogradoff, D, Bui, M, Dalal, Y, and Papoian, GA (2016). Promiscuous Histone Mis-Assembly Is Actively Prevented by Chaperones. J Am Chem Soc.

Zhao, H, Winogradoff, D, Dalal, Y, and Papoian, GA (2019). The Oligomerization Landscape of Histones. Biophys J.

Zhu, J, Cheng, KCL, and Yuen, KWY (2018). Histone H3K9 and H4 Acetylations and Transcription Facilitate the Initial CENP-AHCP-3Deposition and de Novo Centromere Establishment in Caenorhabditis elegans Artificial Chromosomes. Epigenetics and Chromatin.

Figures

Figure 1

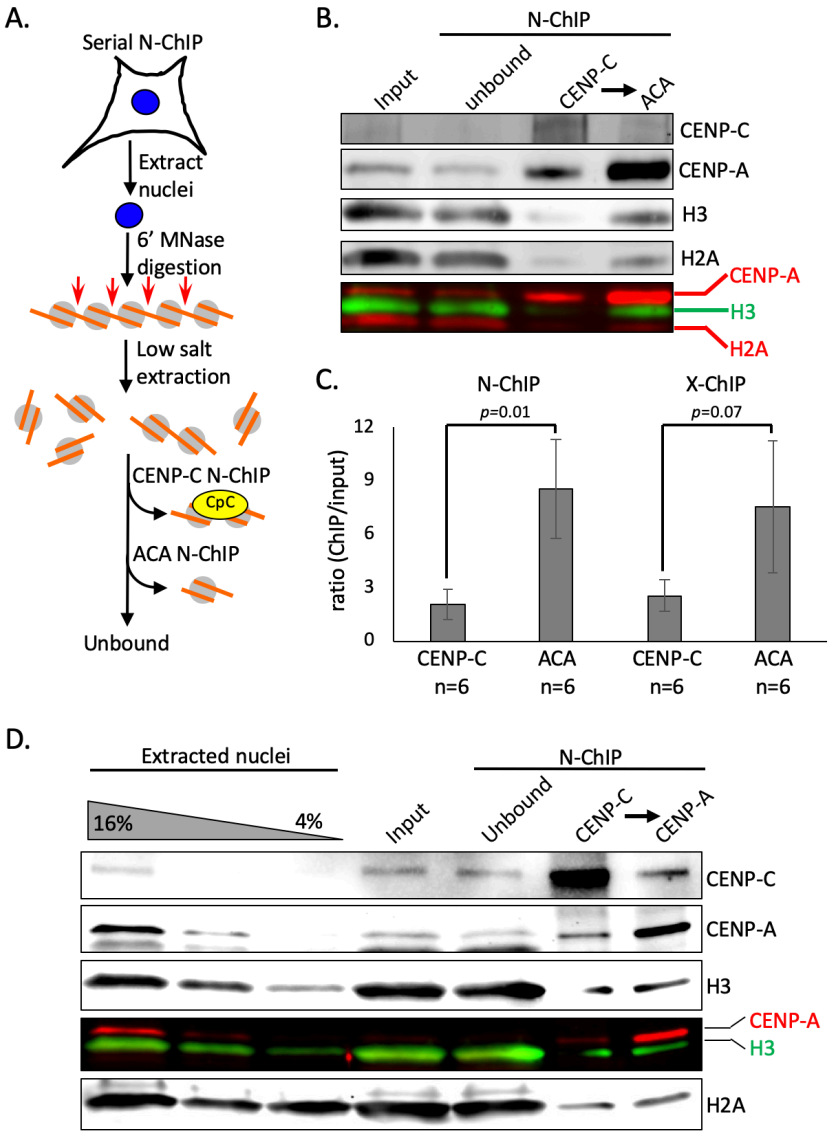

Figure 1. CENP-C binds a subset of CENP-A nucleosomes

(A) Schematic of experimental set-up of serial chromatin immunoprecipitation. (B) Western blot analysis of the serial N-ChIP was performed and probed for H2A, H3, CENP-A, and CENP-C. (C) Quantification of CENP-A enrichment in either CENP-C or subsequent ACA N-ChIP or X-ChIP confirms the presence of two CENP-A populations (paired t-test; significance was determined at $p<0.05$). (D) A serial dilution of extracted nuclei was loaded side-by-side to a CENP-C N-ChIP followed by a CENP-A N-ChIP.

Figure 2

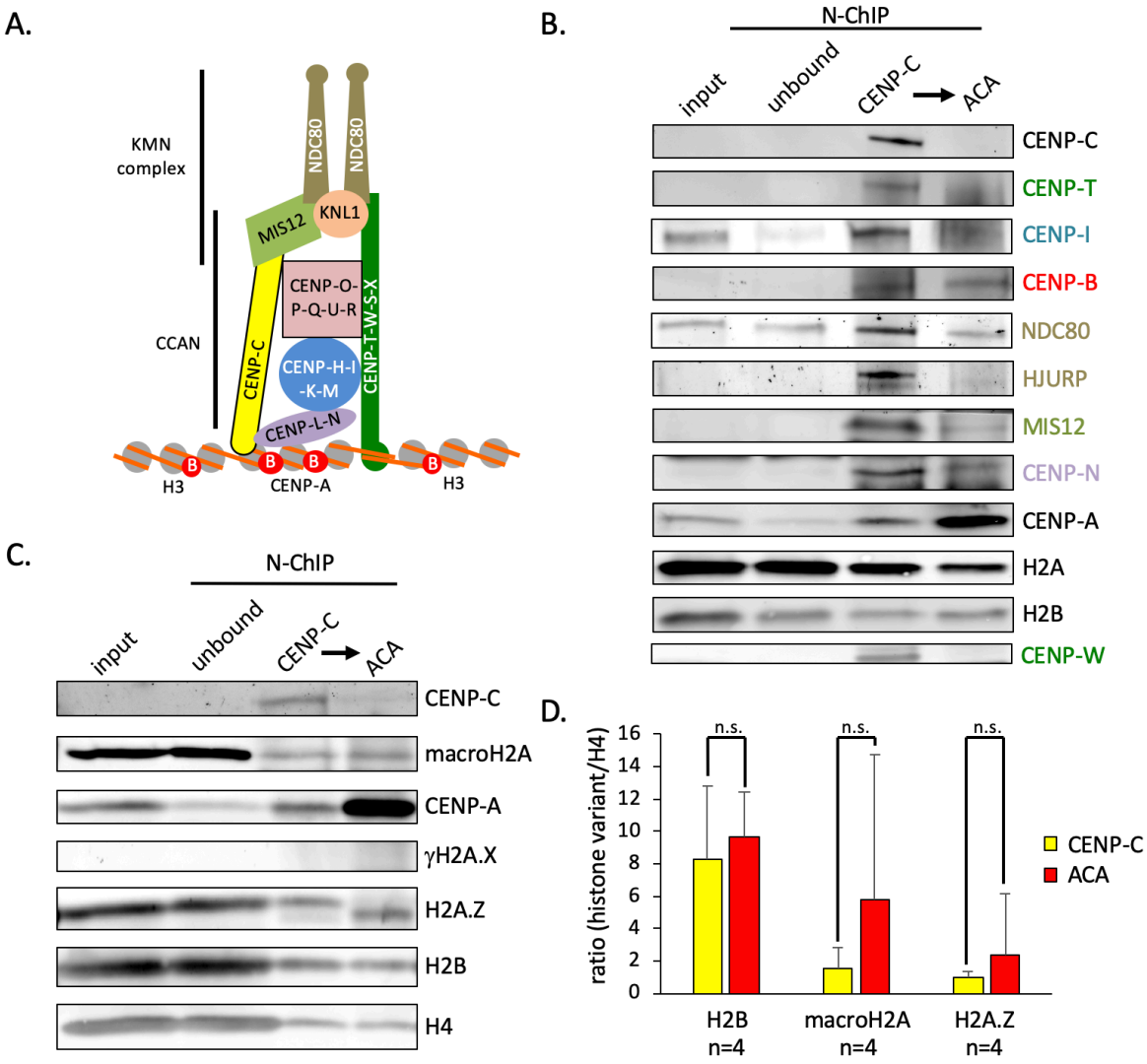

Figure 2. A small fraction of CENP-A stably associates with the inner kinetochore

(A) To determine if CENP-C N-ChIP also brought down kinetochore components, both CENP-A populations were purified and probed for the histones (H2A, H4, CENP-A), CENP-B, inner kinetochore components (CENP-W, CENP-T, CENP-I, CENP-N), and outer kinetochore components (MIS12, HEC1). (C) To determine whether histone H2A variants associate with CENP-A nucleosomes in complex with CENP-C or bulk CENP-A, we performed western blot analysis probing for γH2A.X, H2A.Z, and macroH2A. (D) Quantification of four independent experiments revealed that none of the H2A variants was enriched in either CENP-A population. As a control, we measured the relative amount of H2B over H4 (paired t-test; significance was determined at $p<0.05$).

Figure 3

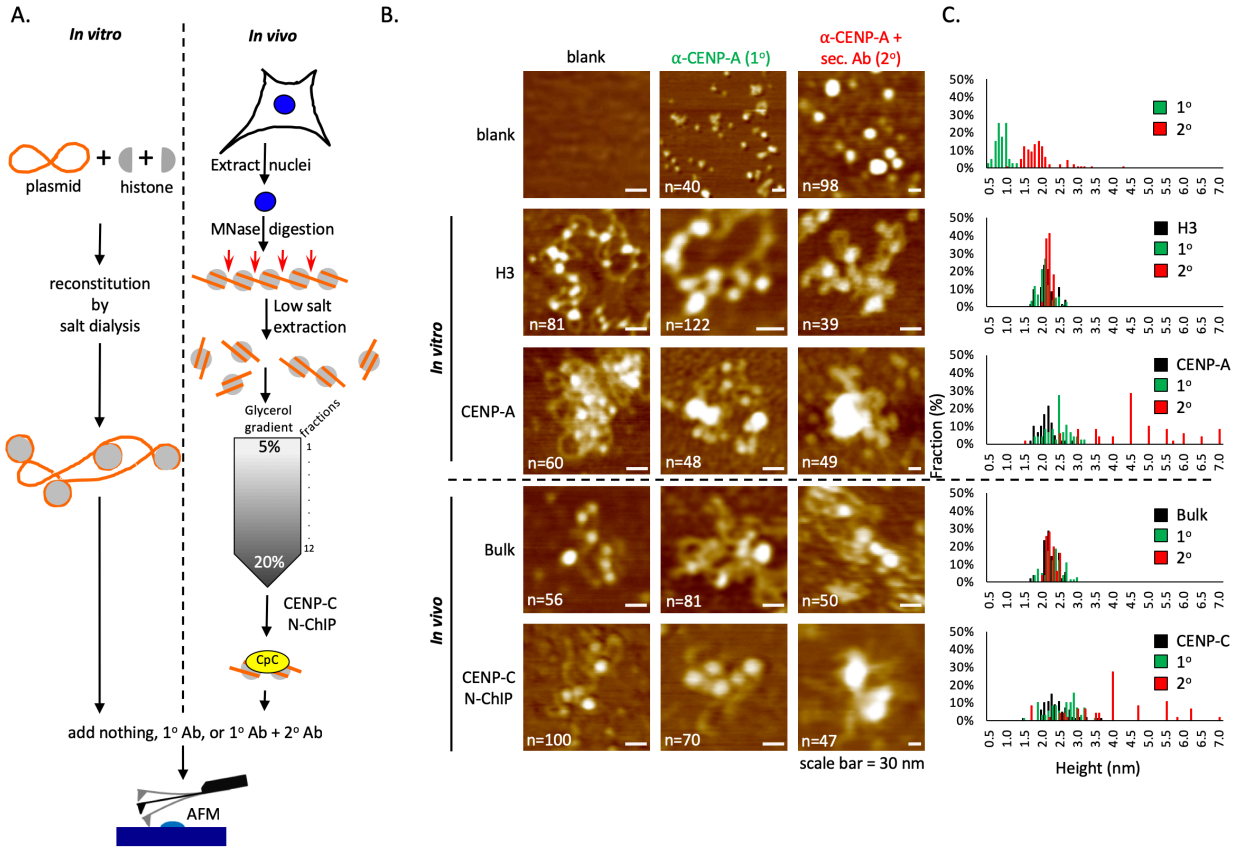

Figure 3. Immuno-AFM confirms CENP-C associates with CENP-A nucleosomes

(A) To confirm that CENP-C associated with CENP-A nucleosomes, we performed immuno-AFM on *in vitro* reconstituting H3 and CENP-A nucleosomes in parallel to extracted bulk and CENP-C associated chromatin. (B) Representative images for three conditions (no antibody, 1° antibody, 1° plus 2° antibodies) per sample. The scale bar is 30 nm. (C) Height measurement of all three conditions were plotted per sample, showing that anti-CENP-A antibody only recognized *in vitro* reconstituted CENP-A nucleosomes and nucleosomes associated with CENP-C, confirming that CENP-C indeed strongly associated with CENP-A nucleosomes.

Figure 4

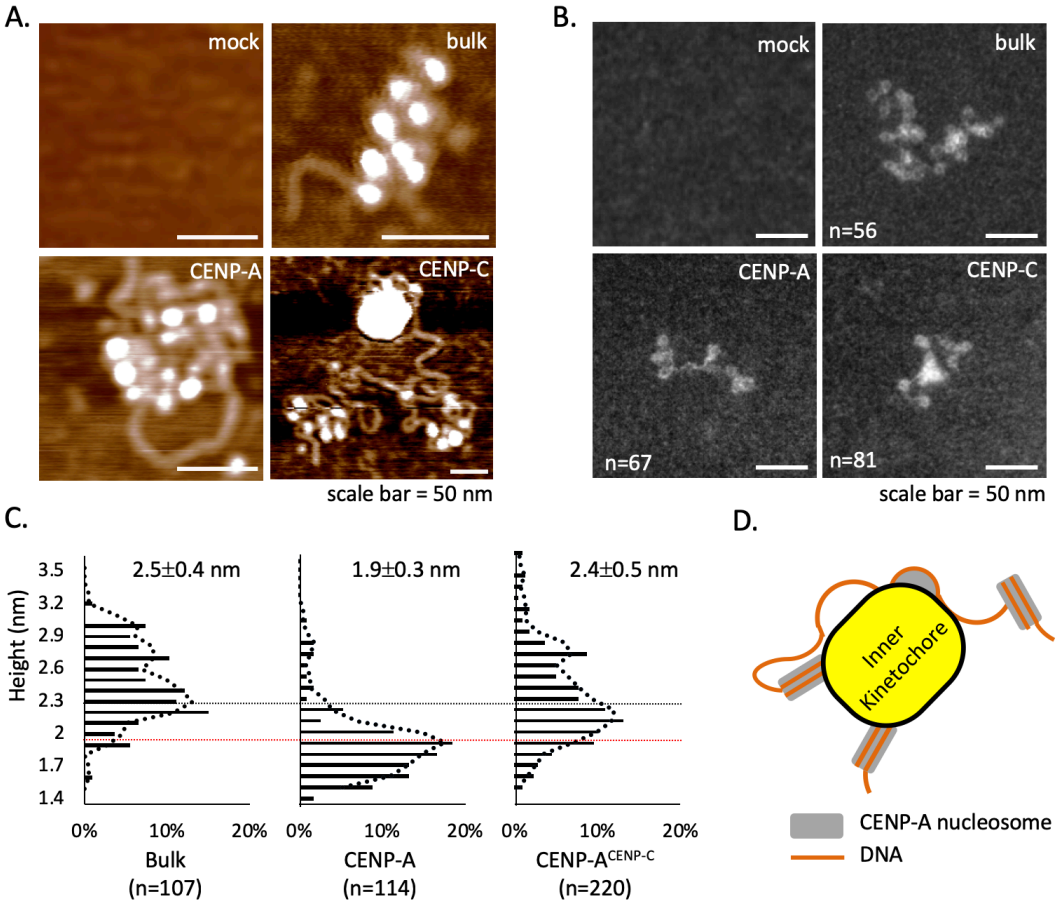

Figure 4. Purified CENP-C complex are associated with stable octameric CENP-A nucleosomes

Chromatin was extracted from HeLa cells after 6-minute MNase digestion, followed by either mock, CENP-A, or CENP-C N-ChIP. Unbound chromatin was used for bulk chromatin. Representative AFM (A) and TEM (B) images of either mock, bulk chromatin, CENP-A chromatin, or CENP-C chromatin showed that CENP-C complex is a large polygonal structure. (C) Nucleosomal height was quantified for either bulk chromatin, CENP-A, or CENP-A nucleosomes associated with CENP-C complex. The mean height with standard error is shown, as well as their distribution. Robustly kinetochore associated CENP-A nucleosomes were significantly taller than weakly or not bound CENP-A nucleosomes (2-sided t test $p<2.6\cdot10^{-18}$). (D) A model showing how 4-6 CENP-A nucleosomes associate with the inner kinetochore, including a stretch of 230-bp of naked DNA that is refractory to MNase digestion.

Figure 5

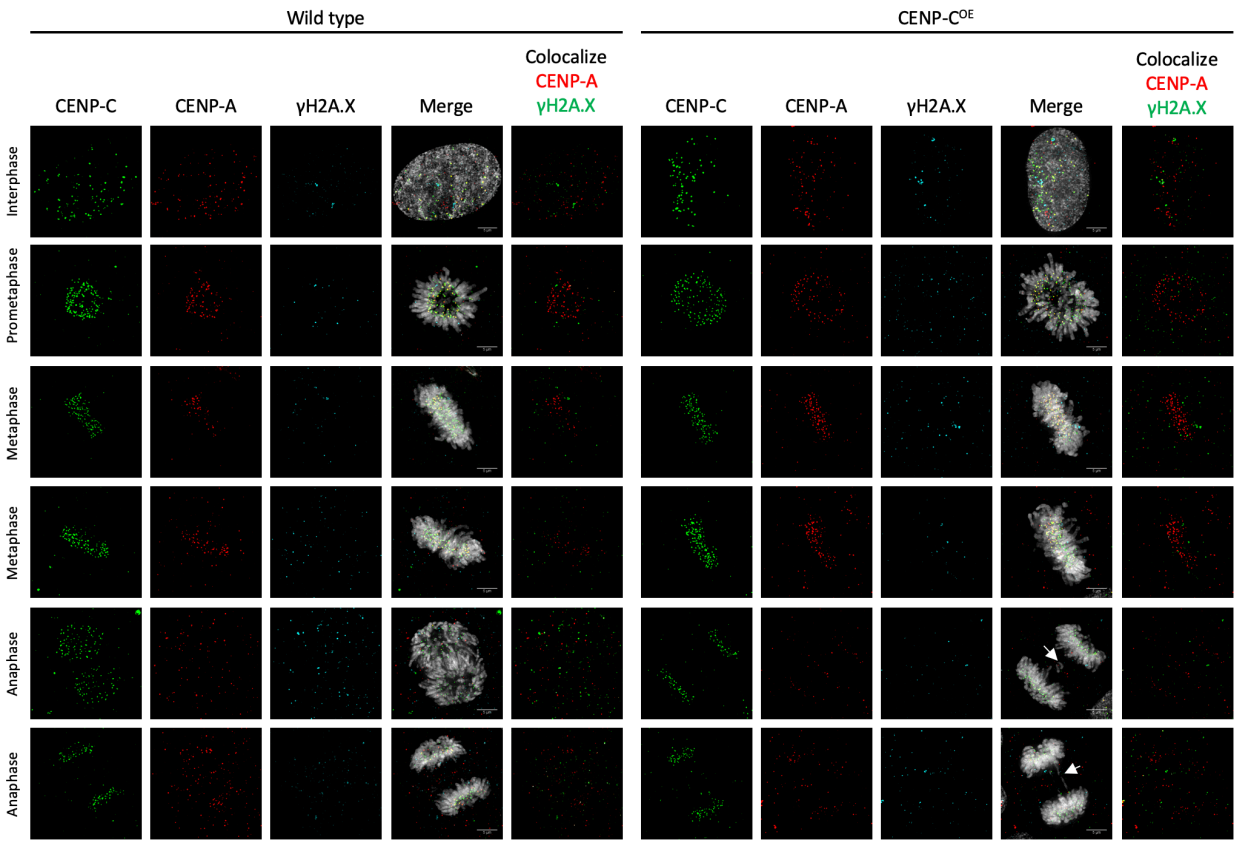

Figure 5 – CENP-C overexpression did not increase mitotic double strand DNA breaks

Representative images of either wild-type or CENP-C overexpressing HeLa cells. HeLa cells were transfected for three days and synchronize to early G1 prior to fixation and staining for CENP-C (green), CENP-A (red), γH2A.X (cyan), and DAPI (grey). No difference in number of γH2A.X foci was observed between the two samples. Arrow highlight lagging chromosomes.

Figure 6

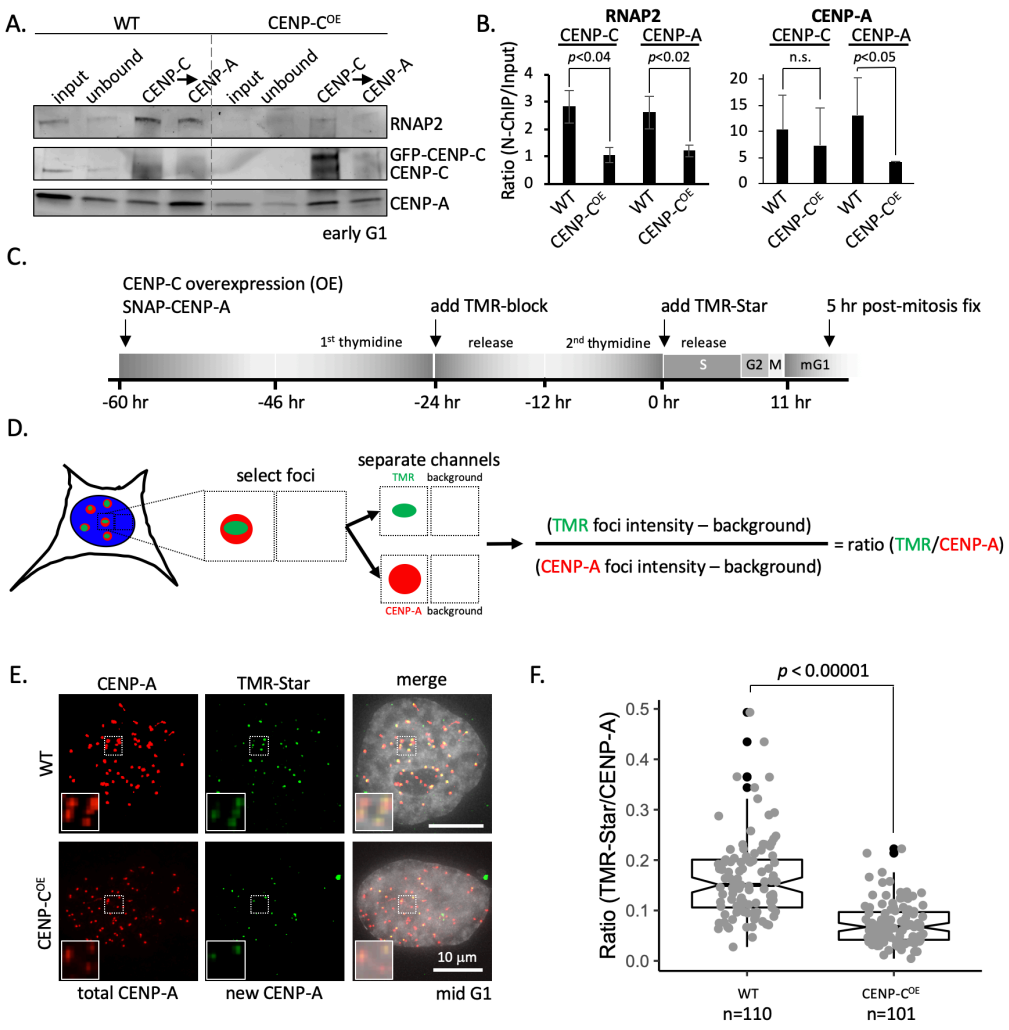

Figure 6. New CENP-A loading impaired upon CENP-C overexpression

(A) Western blot comparing wild-type versus CENP-C^{OE} conditions for RNAP2, CENP-C, and CENP-A levels at early G1. (B) Quantification of RNAP2 and CENP-A levels. (C) Schematic of experimental design. (D) Colocalizing immunofluorescent signal for CENP-A and TMR-Star are collected and the intensity of both foci is measured as well as background directly neighboring the foci to determine the ratio TMR-star signal over total CENP-A signal. (E) *De novo* CENP-A incorporation was assessed by quench pulse-chase immunofluorescence. After old CENP-A was quenched with TMR-block, newly loaded CENP-A was stained with TMR-Star and foci intensity was measured over total CENP-A foci intensity. Inset is a 2x magnification of the dotted box in each respective image. (F) Quantification of *de novo* CENP-A loading by measuring the ratio of TMR-Star signal over total CENP-A signal.

Figure 7

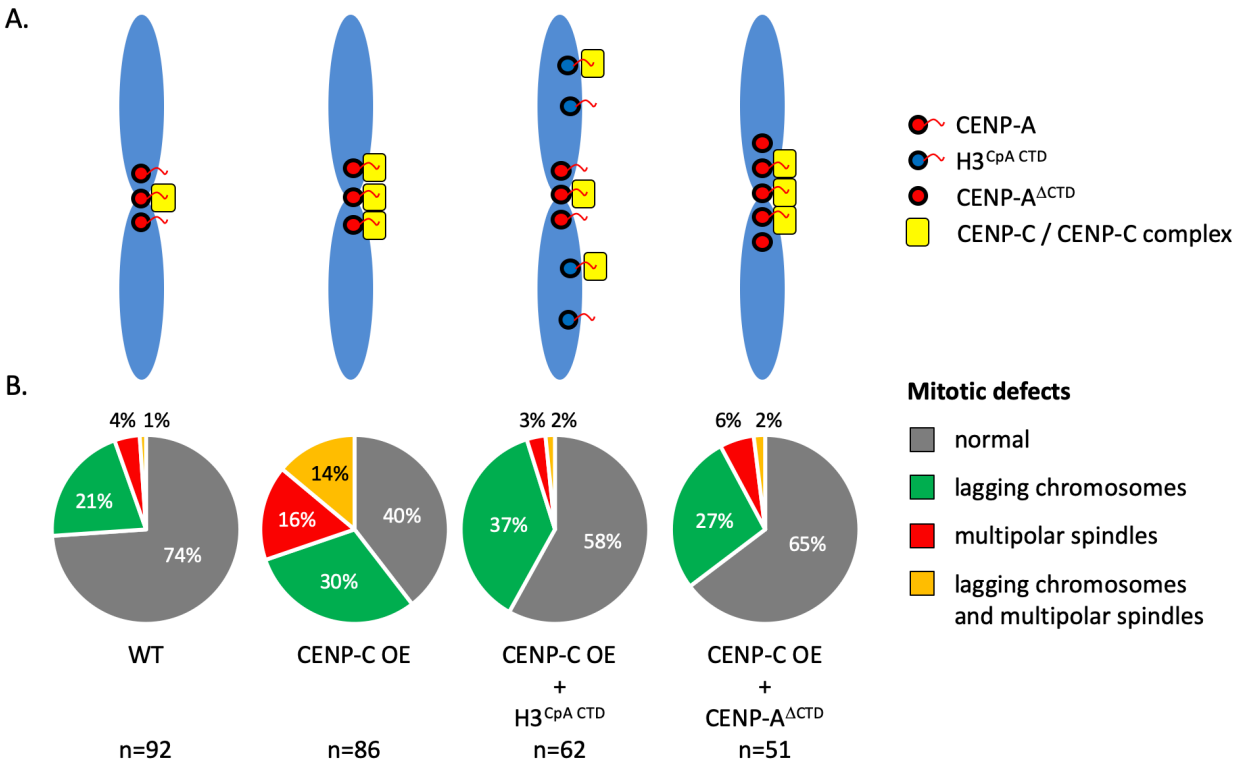

Figure 7. CENP-C overexpression leads to increased mitotic defects, which can be rescued with CENP-A CTD mutants

(A) Three days of ectopic overexpression of CENP-C, which were synchronized to M phase, resulted in dramatic increase in mitotic defects compared to wild-type cells. The C-terminal tail of CENP-A is essential for recruitment of CENP-C. We reasoned that to rescue the mitotic defect of CENP-C overexpression by co-expressing histone H3 with the C-terminal tail of CENP-A ($H3^{CpA\ CTD}$) or CENP-A lacking its C-terminal tail ($CENP\text{-}A^{\Delta CTD}$). (B) Mitotic defects were quantified. We observed that the level of both multipolar spindle (red) and multipolar spindle with lagging chromosome (orange) were reduced to wild-type levels.

Supplemental Figures

Supplemental Figure S1

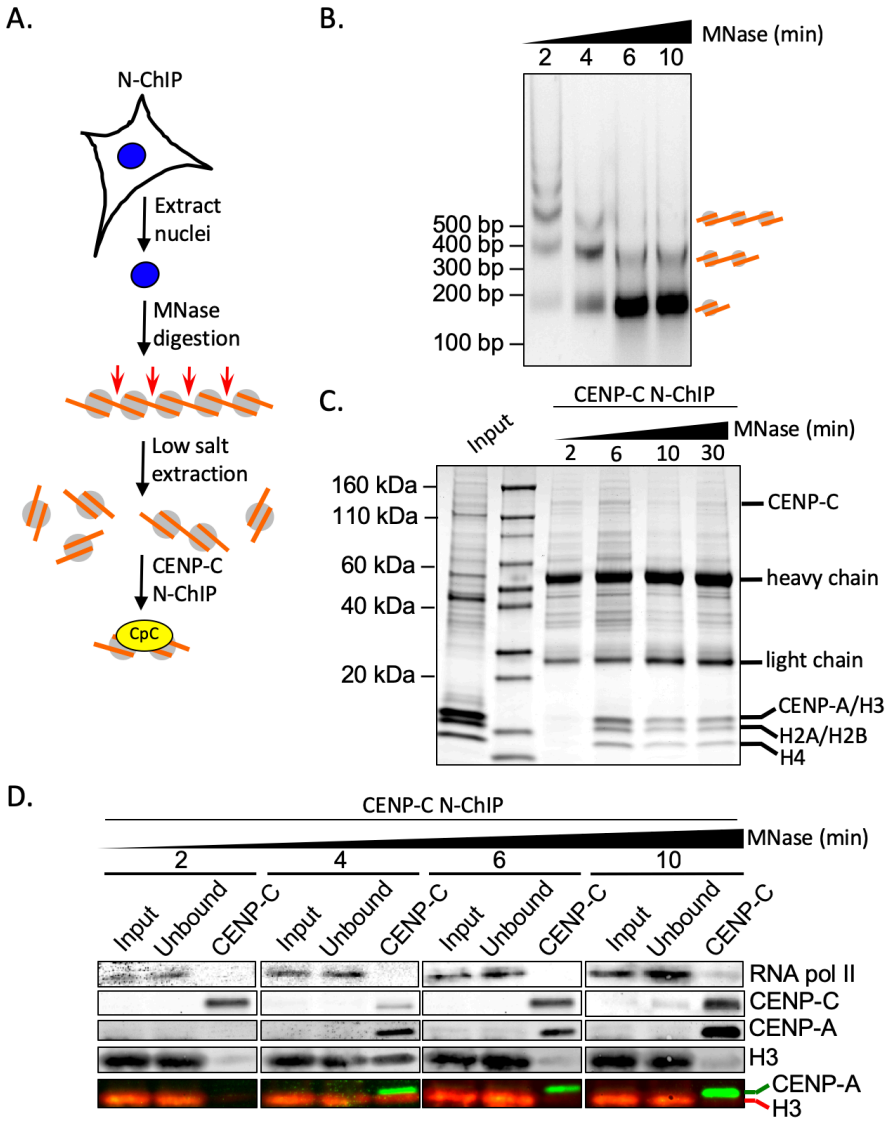

Supplemental Figure S1. CENP-C N-ChIP efficiently pulls down CENP-A nucleosomes

(A) Diagram of experimental protocol for purifying CENP-C associated chromatin. (B) DNA products followed a time course of MNase digestion were resolved on a 1% agarose gel. (C) CENP-C N-ChIP samples obtained from a MNase digestion time course were resolved on 4-20% SDS Page and stained with total protein. (D) Western blot analysis of CENP-C ChIP following a MNase time course showed that after 6-minute MNase digestion, CENP-C ChIP almost exclusively pulls down CENP-A nucleosomes.

Supplemental Figure S2

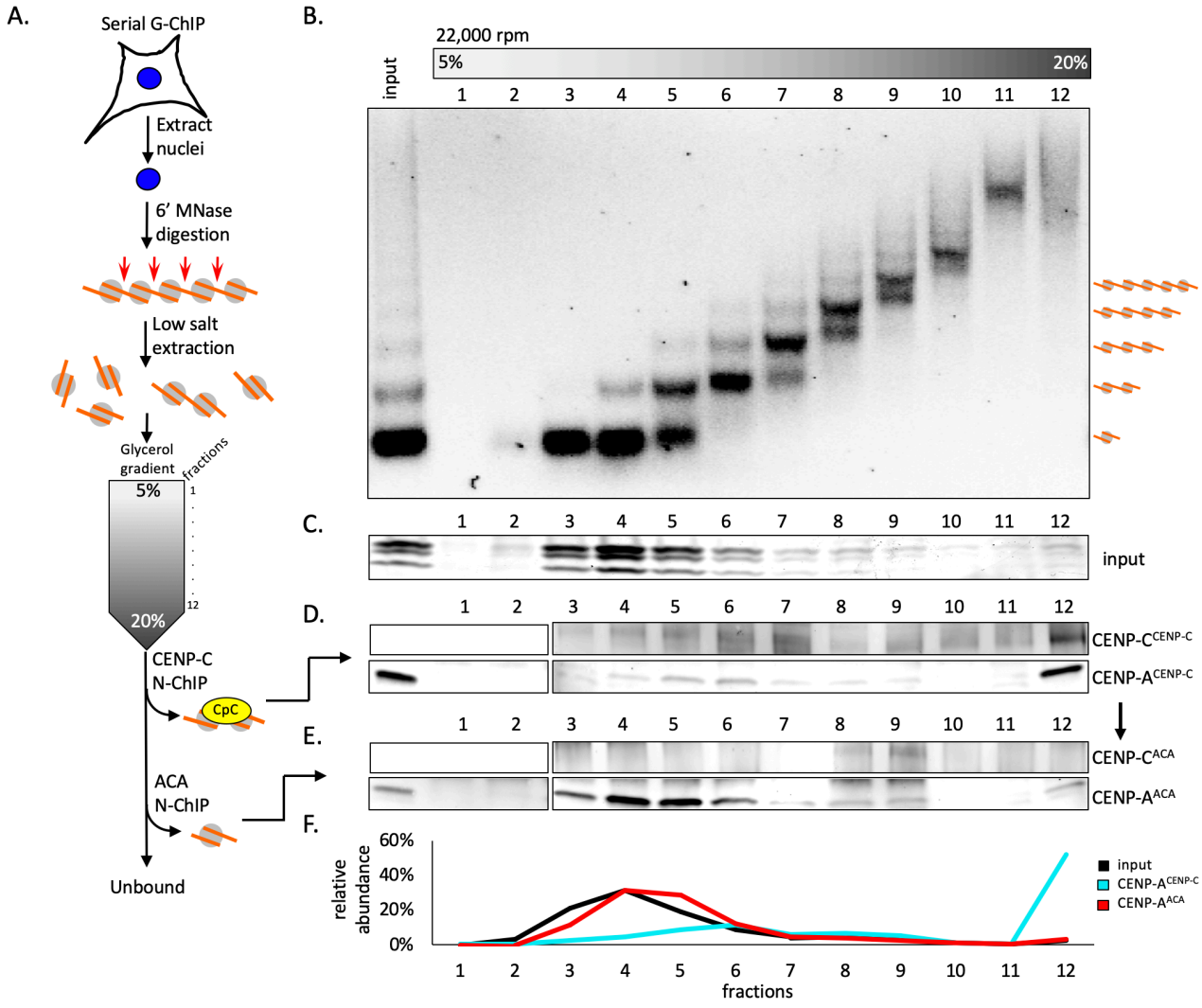

Supplemental Figure S2. Two distinct classes of CENP-A nucleosome are found at the centromere

(A) Extracted chromatin was separated by a 5-20% glycerol gradient sedimentation assay from which twelve one mL fractions were isolated. (B) DNA from 50 µL aliquots per fraction was isolated and run on a 1.2% agarose gel. (C) Each fraction was run on an SDS-PAGE gel to determine the relative histone content. (D) Following CENP-C N-ChIP and (E) the subsequent serial ACA N-ChIP, each fraction was probed for CENP-C and CENP-A. (F) Quantification of relative histone levels from (C) or relative CENP-A levels from (D) and (E) per fraction are plotted. All experiments were performed in triplicates.

Supplemental Figure S3

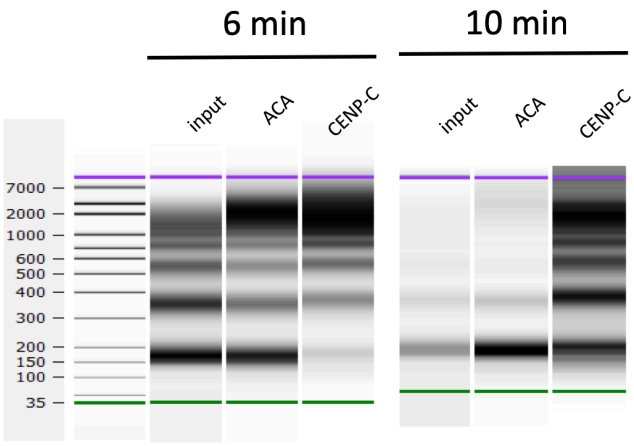

Supplemental Figure S3. CENP-C associated chromatin is more refractory to MNase digestion than ACA chromatin

Bulk chromatin and both CENP-A populations were purified by N-ChIP from HeLa cells following either 6 or 10 minute MNase digestion and analyzed on the BioAnalyzer. CENP-C associated chromatin showed greater protection from MNase digestion compared to bulk or ACA chromatin.

Supplemental Figure S4

A.

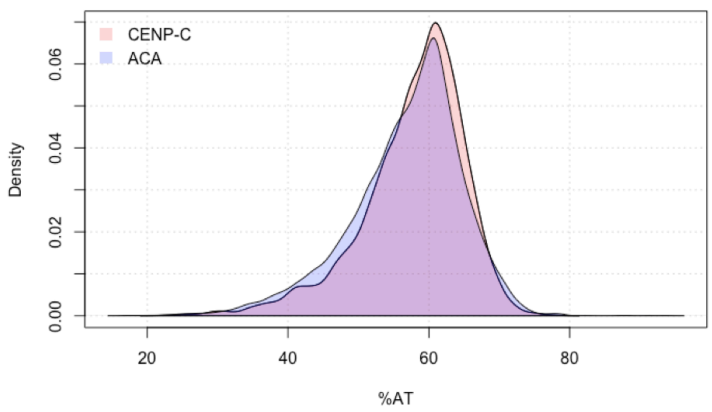

B.

	ACA		CENP-C	
Monomers	**Count**	**Fraction**	**Count**	**Fraction**
ALR	35	3.12%	6	2.80%
ALR1	60	5.35%	10	4.67%
ALR2	17	1.52%	12	5.61%
Hasson	457	40.77%	90	42.06%
Henikoff_Cen1	454	40.50%	76	35.51%
Henikoff_Cen13	98	8.74%	20	9.35%
Total	**1121**	**100.00%**	**214**	**100.00%**

Supplemental Figure S4. Both CENP-A populations occupy essentially the same

The obtained PacBio sequence reads from either CENP-C or subsequent ACA N-ChIP-seq were first compared for their AT content as a first estimate if these two CENP-A populations might occupy different sequences. Second, the sequence reads were aligned to established centromeric α-satellite sequences. In both cases no differences were observed. ALR, ALR1, and ALR2 are α-satellite DNA from RepBase, Hasson is based on the sequence used by (Hasson *et al.*, 2013), Henikoff_Cen1 and Henikoff_Cen13 were derived from (Henikoff *et al.*, 2015).

Supplemental Figure S5

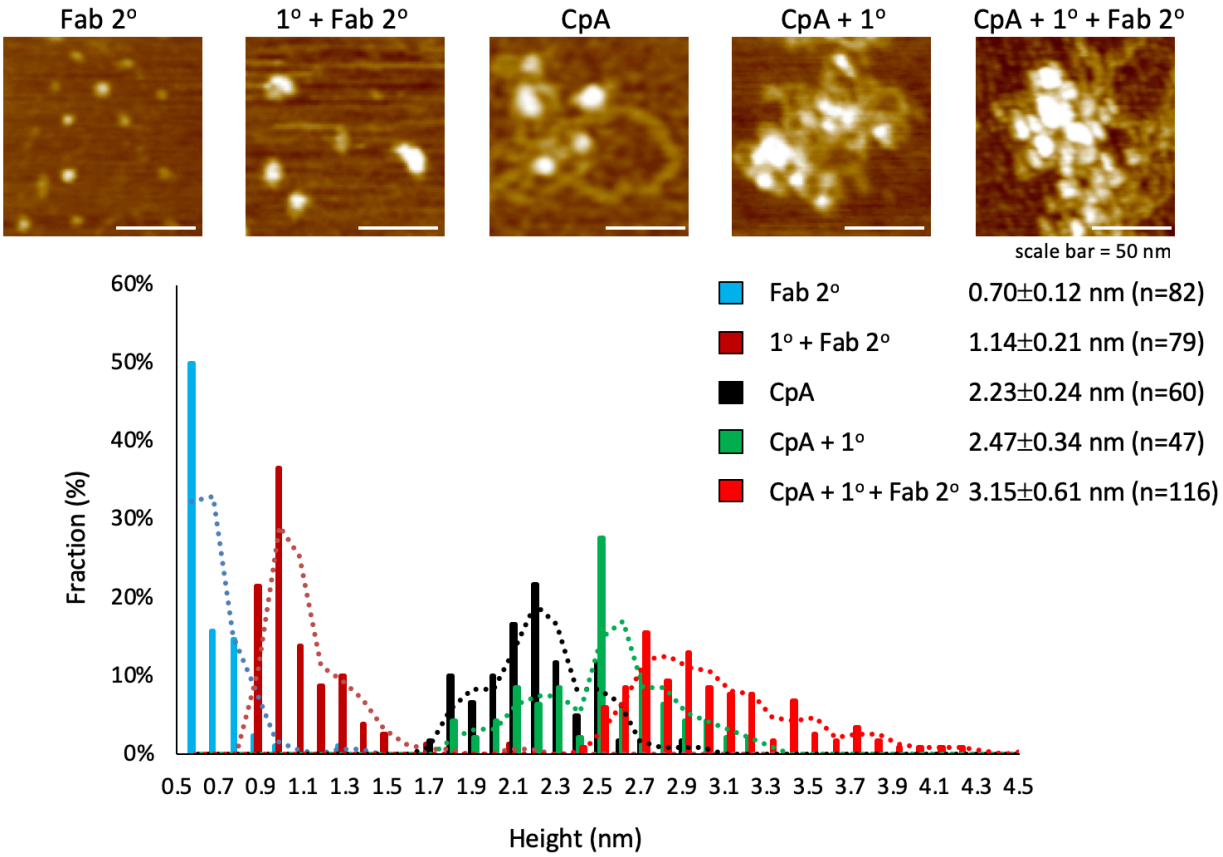

Supplemental Figure S5. Immuno-AFM confirms CENP-A nucleosome identity by Fab fragment.

To confirm that the secondary antibodies used in Figure 3 did not result in aberrant confirmation due to clustering induced by the secondary antibodies, we also confirmed CENP-A nucleosome identity using the anti-mouse Fab fragment.

Supplemental Figure S6

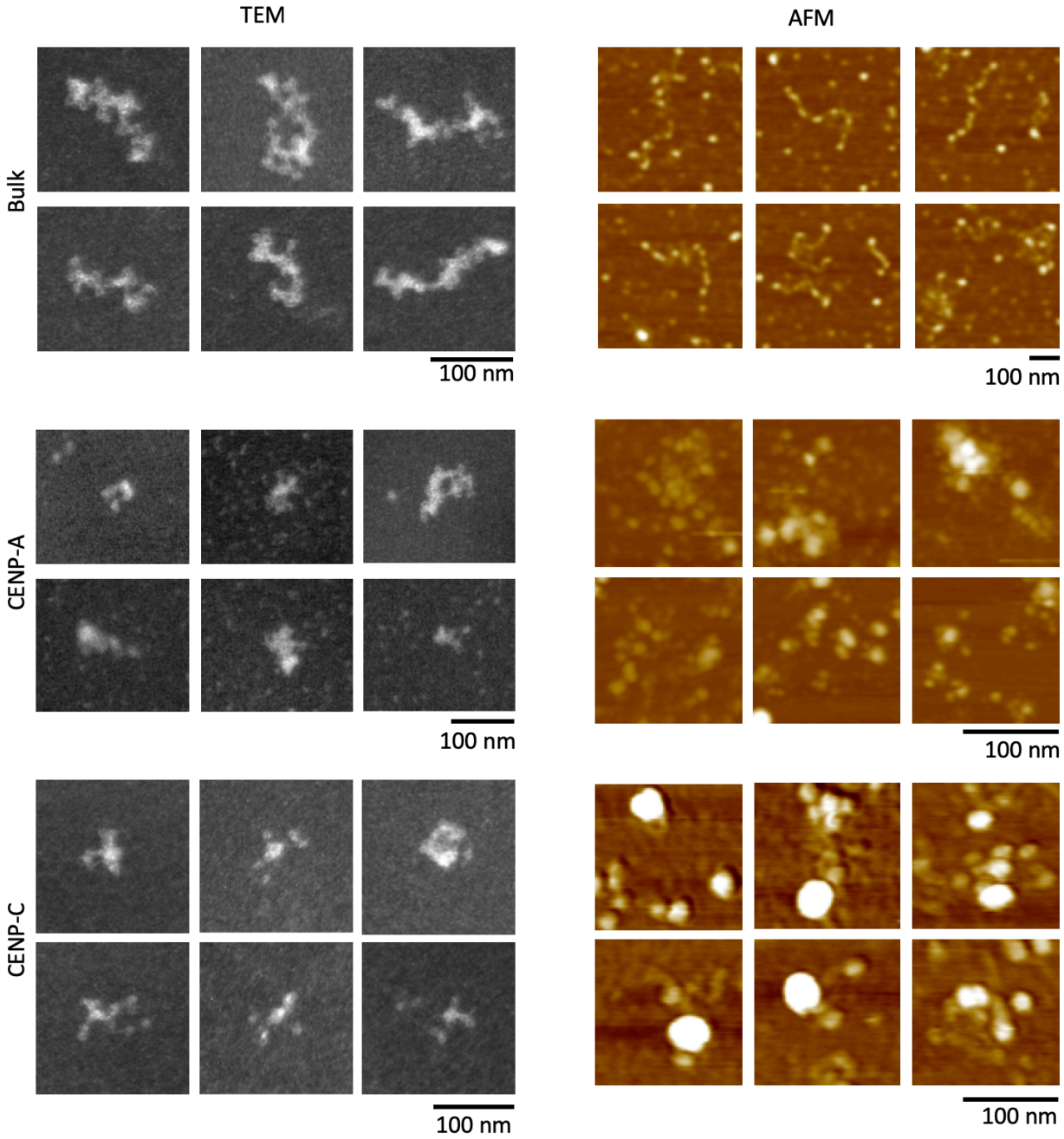

Supplemental Figure S6. Representative TEM and AFM images of bulk, CENP-A, and CENP-C chromatin

For each condition, six representative images are shown. The scale bar is 100 nm.

Supplemental Tables

Supplemental Table S1. Quantification of CENP-A levels for the two CENP-A populations From HeLa cells, native centromeric chromatin was isolated by serial CENP-C and ACA N-ChIP. CENP-A levels were quantified from Western blot. 6-11 independent replicates were quantified using LiCor software. Quantification of CENP-C or ACA over input demonstrated that under native ChIP conditions, 6-fold excess of weakly bound CENP-A exist over robustly bound CENP-A, whereas under cross-linked ChIP conditions, an almost two-fold excess was found. Overall, these analyses confirm that two distinct and sizable CENP-A populations exist in cycling human cells. Values are a.u.

Table S1: A sizable fraction of CENP-A chromatin is not strongly associated with CENP-C						
N-ChIP quantification for Figures 1C						
	input	**CENP-C IP**	**ACA IP**	**CENP-C/input**	**ACA/input**	**ACA/CENP-C**
Exp1	0.91	2.30	14.7	2.52	16.12	6.39
Exp2	0.56	3.34	10.0	5.95	17.83	2.99
Exp3	26.6	13.4	57.8	0.50	2.17	4.31
Exp4	26.0	15.2	81.3	0.58	3.13	5.35
Exp5	7.00	9.76	43.8	1.39	6.26	4.49
Exp6	9.07	11.8	52.3	1.30	5.77	4.43

X-ChIP quantification for Figures 2C						
	input	**CENP-C IP**	**ACA IP**	**CENP-C/input**	**ACA/input**	**ACA/CENP-C**
Exp1	7.50	21.4	42.8	2.85	5.71	2.00
Exp2	6.98	13.3	21.7	1.91	3.11	1.63
Exp3	7.71	0.86	3.37	0.11	0.44	3.92
Exp4	3.44	7.66	17.6	2.23	5.12	2.30
Exp5	1.44	2.18	7.41	1.51	5.15	3.40
Exp6	0.31	2.05	7.96	6.61	25.68	3.88

	N-ChIP		**X-ChIP**	
	CENP-C/input	**ACA/input**	**CENP-C/input**	**ACA/input**
mean	2.04	8.54	2.54	7.53
median	1.35	6.01	2.07	5.13
stdev	2.05	6.73	2.20	9.10
SE	0.84	2.75	0.90	3.71
Paired t test		0.012		0.070

Supplemental Table S2. Quantification of histone H2A variants levels for the two CENP-A populations

From HeLa cells, native centromeric chromatin was isolated by serial CENP-C and ACA N-ChIP. CENP-A levels were quantified from Western blot. 4 independent replicates were quantified using LiCor software. Quantification of H2B, macroH2A, and H2A.Z over H4 demonstrated that under native ChIP conditions, no significant enrichment was observed between either CENP-C or the serial ACA N-ChIP. Values are a.u.

Table S2. Histone H2A variants are not relatively enriched in either CENP-A population								
	CENP-C IP				ACA IP			
	H4	macroH2A	H2AZ	H2B	H4	macroH2A	H2AZ	H2B
Exp1	2.9	2.43	3.58	30.1	2.35	1.76	2.59	23.2
Exp2	1.43	2.21	2.07	29.7	1.69	1.45	3.04	22.3
Exp3	2.47	2.92	0.83	1.67	0.136	5.19	2.34	1.99
Exp4	0.512	3.27	0.99	1.07	0.595	14.4	2.73	1.53
mean	1.83	2.71	1.87	15.64	1.19	5.7	2.68	12.26
median	1.95	2.68	1.53	15.69	1.14	3.48	2.66	12.15
stdev	1.07	0.48	1.27	16.47	1.01	6.04	0.29	12.13
SE	0.54	0.24	0.63	8.24	0.51	3.02	0.015	6.06
	Ratio histone variant over H4							
	CENP-C				ACA			
		macroH2A/H4	H2AZH4	H2B/H4		macroH2A/H4	H2AZH4	H2B/H4
Exp1		0.84	1.23	10.38		0.75	1.10	9.87
Exp2		1.55	1.45	20.77		0.86	1.80	13.20
Exp3		1.18	0.34	0.68		38.16	17.21	14.63
Exp4		6.39	1.93	2.09		24.20	4.59	2.57
mean		9.95	4.95	33.91		63.97	24.70	40.27
median		1.36	1.34	6.23		12.53	3.19	11.53
stdev		2.62	0.67	9.24		18.44	7.51	5.38
SE		1.31	0.33	4.62		9.22	3.75	2.69
Paired t test						0.114	0.154	0.374

Supplemental Table S3. Quantification of immuno-AFM measurements

In order to assess whether CENP-C would associate with CENP-A nucleosomes, immuno-AFM was used on both in vitro reconstituted H3 and CENP-A nucleosomes, as well as bulk chromatin and CENP-C ChIP'ed chromatin from HeLa cells. In vitro reconstituted H3 nucleosomes did not change in height upon exposure to anti-CENP-A antibody or the combination of anti-CENP-A + anti-mouse secondary antibody. In contrast, CENP-A nucleosomes did change height substantially (Figure 5). Using an anti-mouse Fab fragment also showed a change in height of CENP-A nucleosomes (Figure S4). Finally, bulk chromatin was purified from HeLa cells, but did not show change in nucleosome height upon exposure to either anti-CENP-A antibody or anti-CENP-A antibody + anti-mouse secondary antibody. Nucleosomes associated with the CENP-C complex did, thereby confirming the identity of the associated nucleosomes as CENP-A nucleosomes.

Table S3. Quantification of immuno-AFM to identify CENP-A nucleosomes in CENP-C associated chromatin											
					In vitro reconstituted nucleosomes						
					H3 nucleosome			**CENP-A nucleosome**			
1° antibody	X	X		X		X	X		X	X	X
2° antibody		X					X			X	
2° Fab			X	X							X
N	40	99	82	79	81	122	37	60	48	49	120
mean (nm)	0.9	2	0.7	1.1	2.2	2.1	2.2	2.2	2.5	4.6	3.2
stdev	0.2	0.5	0.1	0.2	0.2	0.2	0.1	0.2	0.3	1.4	0.6

					In vivo purified chromatin					
					bulk chromatin			**CENP-C chromatin**		
1° antibody						X	X		X	X
2° antibody							X			X
2° Fab										
N					56	81	50	100	70	49
mean (nm)					2.3	2.4	2.3	2.4	2.6	3.9
stdev					0.2	0.3	0.1	0.4	0.4	1.3

Supplemental Table S4. Quantification of CENP-C complex dimensions and refractory naked DNA.

CENP-C chromatin was isolated from HeLa cells and imaged by in air AFM by non-contact tapping mode. The height and surface area dimensions were obtained. In addition, frequently a DNA loop was observed coming out of the CENP-C complex. By ImageJ these stretches of DNA were measured.

Table S4. Measurements of CENP-C complex dimensions and lengths of associated DNA loop		
CENP-C complex dimensions		
mean height (nm)	5.57	N=177
median height (nm)	4.95	
stdev	2.05	
mean area (nm^2)	629	N=177
median area (nm^2)	540	
stdev	358	
Length of naked DNA loop		
mean length (bp)	232.9	N=44
median length (bp)	148.5	
stdev	267.2	

Supplemental Table S5. CENP-C associated CENP-A nucleosomes have octameric dimensions.

From HeLa cells CENP-A and CENP-C chromatin were purified. The unbound fraction was used as bulk control. Chromatin was visualized by in air AFM in non-tapping contact mode. Nucleosomal height was determined by ImageJ as well as manual spot checking.

Table S5. Nucleosomal height of bulk, CENP-C associated CENP-A nucleosomes, and CENP-A nucleosomes			
	***In vivo* extracted chromatin**		
	bulk	**CENP-A**	**CENP-C**
N	107	114	220
mean height (nm)	2.5	1.9	2.4
median height (nm)	2.5	1.9	2.3
stdev	0.3	0.3	0.45
SE	0.03	0.03	0.03
Two-sided t test			2.64E-18

Supplemental Table S6. CENP-C associated CENP-A nucleosomes have octameric dimensions.

From HeLa cells that were either transfected with mock or GFP-CENP-C plasmids and synchronized to early G1. Chromatin was extracted as described in Figure 1A. Western blot analysis was performed as described in Methods and probed for RNAP2 and CENP-A. The bands of three independent experiments were measured using LiCor's software.

Supplemental Table S6: Quantification of band intensity of RNA polymerase 2 and CENP-A western blots. Values are arbitrary units derived from LiCor's software (10^3).								
RNAP2								
	WT					**CENP-C overexpression**		
	Input	**CENP-C**	**ACA**			**Input**	**CENP-C**	**ACA**
Exp1	7.73	28.8	21.8		**Exp1**	3.12	4.31	3.36
Exp2	8.99	16.4	17.6		**Exp2**	2.79	2.40	4.08
Exp3	6.73	19.7	20.8		**Exp3**	1.95	1.80	2.21
		Ratio CpC/input	**Ratio ACA/input**				**Ratio CpC/input**	**Ratio ACA/input**
Exp1		3.73	2.82		**Exp1**		1.38	1.08
Exp2		1.82	1.96		**Exp2**		0.86	1.46
Exp3		2.93	3.09		**Exp3**		0.92	1.13
	mean	2.83	2.62			**mean**	1.05	1.22
	StDev	0.59	0.59			**StDev**	0.28	0.21
CENP-A								
	WT					**CENP-C overexpression**		
	Input	**CENP-C**	**ACA**			**Input**	**CENP-C**	**ACA**
Exp1	0.98	8.63	13.2		**Exp1**	1.97	6.74	8.53
Exp2	0.57	10	11.4		**Exp2**	0.56	8.7	2.18
Exp3	0.38	1.71	2.23		**Exp3**	0.52	1.6	2.02
		Ratio CpC/input	**Ratio ACA/input**				**Ratio CpC/input**	**Ratio ACA/input**
Exp1		8.81	13.47		**Exp1**		3.42	4.33
Exp2		17.54	20.00		**Exp2**		15.54	3.89
Exp3		4.50	5.87		**Exp3**		3.08	3.88
	mean	10.28	13.11			**mean**	7.34	4.04
	StDev	6.65	7.07			**StDev**	7.10	0.25